CM² MAGAZINE

第 50 期

南方科技大学海洋磁学中心主编

创刊词

海洋是生命的摇篮，是文明的纽带。地球上最早的生命诞生于海洋，海洋里的生命最终进化成了人类，人类的文化融合又通过海洋得以实现。人因海而兴。

人类对海洋的探索从未停止。从远古时代美丽的神话传说，到麦哲伦的全球航行，再到现代对大洋的科学钻探计划，海洋逐渐从人类敬畏崇拜幻想的精神寄托演变成可以开发利用与科学研究的客观存在。其中，上个世纪与太空探索同步发展的大洋科学钻探计划将人类对海洋的认知推向了崭新的纬度：深海（deep sea）与深时（deep time）。大洋钻探计划让人类知道，奔流不息的大海之下，埋藏的却是亿万年的地球历史。它们记录了地球板块的运动，从而使板块构造学说得到证实；它们记录了地球环境的演变，从而让古海洋学方兴未艾。

在探索海洋的悠久历史中，从大航海时代的导航，到大洋钻探计划中不可或缺的磁性地层学，磁学发挥了不可替代的作用。这不是偶然，因为从微观到宏观，磁性是最基本的物理属性之一，可以说，万物皆有磁性。基于课题组的学科背景和对海洋的理解，我们对海洋的探索以磁学为主要手段，海洋磁学中心因此而生。

海洋磁学中心，简称 CM^2，一为其全名“Centre for Marine Magnetism”的缩写，另者恰与爱因斯坦著名的质能方程 $E=MC^2$ 对称，借以表达我们对科学巨匠的敬仰和对科学的不懈追求。

然而科学从来不是单打独斗的产物。我们以磁学为研究海洋的主攻利器，但绝不仅限于磁学。凡与磁学相关的领域均是我们关注的重点。为了跟踪反映国内外地球科学特别是与磁学有关的地球科学领域的最新研究进展，海洋磁学中心特地主办 CM^2 Magazine，以期与各位地球科学工作者相互交流学习、合作共进！

“海洋孕育了生命，联通了世界，促进了发展”。 21 世纪是海洋科学的时代，由陆向海，让我们携手迈进中国海洋科学的黄金时代

目 录

磁学演绎.....1

第 40 章 全球铁循环.....1

文献速递.....6

1. 太平洋热带地区台风活动的增加受冰河时代环流变化的驱动.....6

2. 南开海槽俯冲带温度对深部生命的限制.....10

3. 金红石中纳米级的微量元素团簇的地球化学和年代学意义.....13

4. FORC 图的主成分分析方法区分太平洋红层中的生物成因和陆源磁性矿物的组分以及古环境的指示意义.....16

5. 对西非过去 0-2000 AD 地磁场变化的新见解—基于新的 0-2000 AD 古强度曲线.....20

6. 南海神狐区域细粒沉积物粒度特征及其与天然气水合物饱和度的关系..22

7. 磁测定位青铜时代晚期的畜栏.....25

8. 青藏高原是如何动态影响夏季季风降水的?.....27

9. 洞穴沉积物序列中人为产生的灰分层的磁性结构和古地磁分析（Crvena Stijena site, Montenegro）.....29

10. 过去气候变化对未来的启示.....32

11. 对磁铁矿和赤铁矿复杂混合物的磁信号分解技术的评估:犬山红燧石...34

12. 温带地区气候、构造引起的河流演变及岩溶作用和海平面变化的驱动关系.....36

13. 来自南极 Erebus 大火成岩省上新世-更新世的地磁场古方向与古强度结果.....38

磁学演绎

第 40 章 全球铁循环

环境磁学最先通过化学、物理与生物机制与全球“铁循环”联系在一起。铁循环作用于不同的尺度：沙漠粉尘、海洋生物与气候之间的全球性铁联系（Jickells et al., 2005; Maher et al., 2010），有或者没有微生物参与条件下区域性和原地铁氧化物之间的转化（Cornell and Schwertmann, 2003; Malki et al., 2006）。下面我们先简短讨论自然界中全球铁氧化物循环（图 1），然后讨论与环境磁学相关的铁循环物理化学性质。

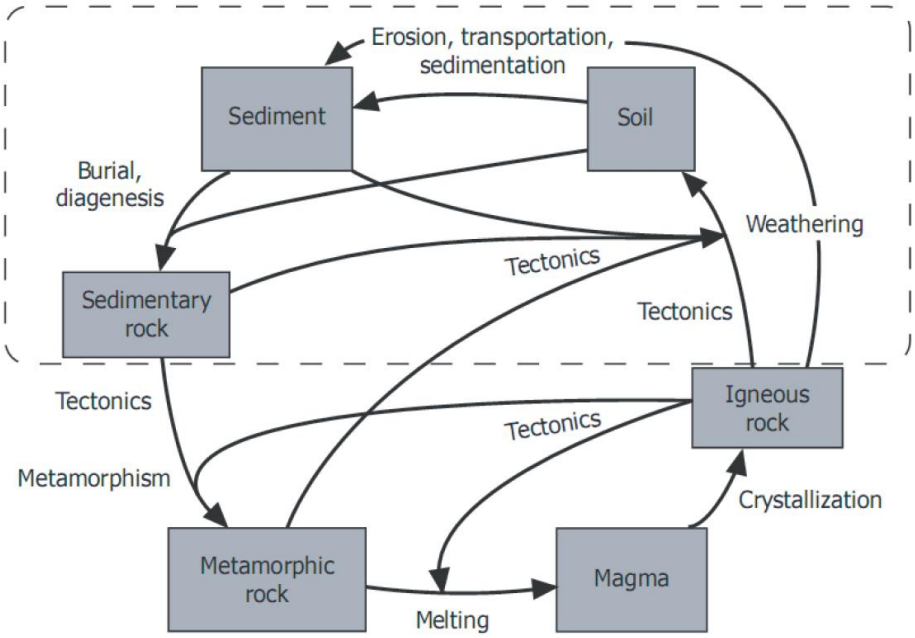

图 1 构造岩石循环 (参考 *Wilson* [1966]和 *Whitmeyer et al.* [2007]). 虚线方框代表环境磁学的主要研究内容

1. 全球铁循环

我们通过研究含铁矿物在岩石中的转化来研究全球铁循环，而岩石中磁性矿物也是环境磁学重要的研究内容（图 1）。磁性矿物在火山岩冷却结晶时形成。磁铁矿在大陆、海洋侵入岩以及深成火山岩中都普遍存在，可能是原生的，也可

能是其他矿物的矿物相变形成（例如，高温氧化、蛇纹石化和水热作用）（Dunlop and Özdemir, 1997）。大陆侵入岩和深成岩中经常含有单斜磁黄铁矿。钛磁铁矿（含有钛磁赤铁矿）一般存在于水成玄武岩，而钛赤铁矿一般存在于长英质火山岩中。侵入岩和深成岩在地壳中缓慢冷却生成的磁性矿物一般颗粒较粗，而喷出岩在地表快速冷却生成的磁性矿物，一般颗粒较细（Dunlop and Özdemir, 1997）。

当火山岩与空气和水开始接触时，它们就开始风化，在地表形成土壤。之前存在的磁性矿物从母岩中释放出来，经过改造形成新的（自生）磁性矿物。土壤中最常见的磁性矿物为磁赤铁矿、针铁矿、赤铁矿和含量很少的磁铁矿。海底玄武岩也会被侵蚀，其中钛磁铁矿往往被氧化成钛磁赤铁矿。当土壤中的原生和自生磁性矿物以及它们的母质受水、冰川和风的侵蚀作用时，它们通过不同的机制，历经不同的时间被搬运，然后沉积在地面（大陆）和水底（海洋和湖泊）（Maher, 2011）。在搬运过程中，磁性矿物通过化学和物理作用被改造，但是母岩中大颗粒的磁性矿物性质在沉积过程中受到的影响很小。

当沉积物被掩埋时，在适当条件下发生的成岩作用通过溶解和重结晶使得碎屑磁性矿物被自生磁性矿物所代替。化学变化贯穿着岩石形成的历史，甚至沉积物岩化形成沉积岩时也在发生。自生矿物在有氧条件下生成磁铁矿和赤铁矿，在缺氧条件下生成磁黄铁矿和胶黄铁矿。埋藏过深或者受到岩浆作用影响都会使沉积岩受到变质作用的影响，根据温度和压力条件的不同，化学性质发生极大的改变。磁铁矿和含量较低的磁黄铁矿是变质岩中最常见的磁性矿物。温度或压力的继续增加，会导致岩石熔化，使得其循环回到起始位置（图 1）。

在地质时期，自然界中不同土壤、沉积物和岩石重复或部分重复着这样的岩石循环，含有与之形成时物理化学条件相对应的磁性矿物。生物作用与矿化过程紧密相连，而且可能是矿化过程的驱动力。生物过程包括在土壤以及沉积物成岩初期有机质的降解和发酵。目前，人类活动在成土作用、沉积物沉积和人工（工业）形成的磁性矿物等各种过程中起到的作用越来越大。环境磁学主要研究控制地球表面或者浅层铁循环的这些过程，主要包含：1）风化和土壤的形成；2)侵蚀、沉积物的沉积和运输（包含有机质，特别是人类和细菌的贡献）；3）沉积物中早期的成岩作用。驱动沉积物中磁性矿物侵蚀、运输和积累的过程，例如铁的物理循环，携带与气候环境及人类活动对环境物理干扰有关的信息。相反，铁的

化学循环主要记录成土作用，成岩作用，生物及人类活动信息，还有它们之中包含的环境信息。除这些过程外，其他的来源也会给沉积物带来磁性矿物，例如通过大气输入的火山灰、人类活动产生的烟尘以及来自太空的粉尘（Suavet et al., 2008）。深海烟囱也是海洋深部可溶金属的重要来源。

2. 磁性矿物中的物理化学铁循环

记录气候、水文和人类活动信息等环境变化的载体有很多，例如，土壤、沉积物和石笋等。环境磁学对这些变化很敏感，这些变化通过铁氧化物（磁铁矿、磁赤铁矿和赤铁矿）、铁的氢氧化物（针铁矿、水铁矿和纤铁矿）、铁的硫化物（胶黄铁矿和磁黄铁矿）和铁的碳酸盐（菱铁矿）等晶格中的 Fe^{2+}和 Fe^{3+}离子沉积或化学变化来实现。Fe^{2+}和 Fe^{3+}离子之间的电子转换对能量要求低（~0.01 eV），很容易发生，每次转换都会导致 1 波尔磁矩（9.27×10^{-24} Am^2）的改变，这些改变发生在化合物不平衡的晶体位中。很多磁学技术手段对这种变化也很敏感，这为揭示环境变化历史提供了高精度的手段（Thompson and Oldfield, 1986）。例如，铁的氧化物或者氢氧化物通过铁离子还原转变成磁铁矿，对追踪土壤铁氧化物类型变化很重要 （Cornell and Schwertmann, 2003; Guyodo et al, 2006a）（图 2）， 因而土壤能携带水文变化、有机质作用或者还原性铁微生物作用的信息（Insam and Domsch, 1988）。类似地，磁铁矿向胶黄铁矿的转化可以携带通过有机质降解形成的还原环境变化信息（e.g., Karlin and Levi, 1983; Canfield and Berner, 1987; Roberts et al., 2011a）。

铁循环是环境变化中沉积记录的一个重要因素。“循环”揭示的是铁离子从一个晶格（针铁矿）到另一个晶格（磁铁矿），当环境条件相反时，铁离子反向迁移也可能发生。环境条件变化可以用这些参数表示：酸度、碱度、化学键强弱、温度、有机碳（C_{org}）或者微化石含量（硅藻、自由硅）。铁循环伴随着电子从 Fe^{2+}到 Fe^{3+}，当 Fe^{2+}（0 K 时 4 个玻尔磁矩）变成 Fe^{3+}（0 K 时 5 个玻尔磁矩），磁化强度增加 25%。确定磁性颗粒粒径的变化能识别这种环境变化，例如铁的还原作用会使土壤表面生成磁化率很高的 SP ($d < 20$ nm)颗粒（*Zhou et al.*, 199）或者稍大的 ARM 很高的 SD 颗粒 (20 nm < d < 1 m)磁铁矿和磁赤铁矿（Liu et al., 2004a）。SD/SP 颗粒的磁性矿物是铁循环强有力的证明。

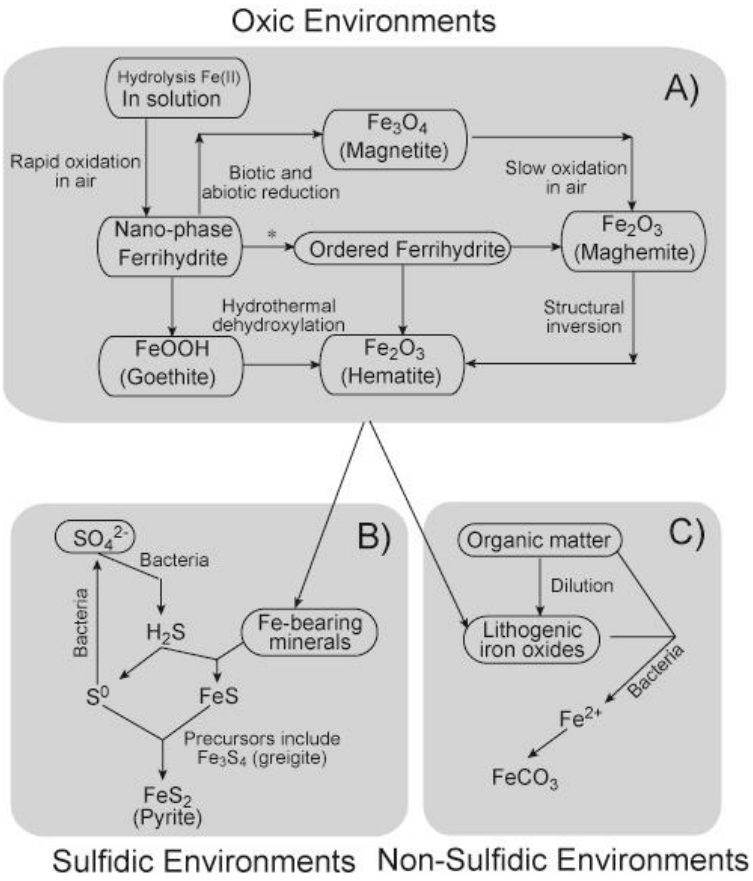

图 2. 铁氧化物和铁硫化物的转化路径（A）在氧化环境中；（B）硫化物环境；（C）非硫化物的厌氧环境。上下的图框内信息分别代表了铁氧化物、铁硫化物和菱铁矿相关的循环反应。其中星号‘*’代表了水铁矿向有序排列的水铁矿转化需要柠檬酸和磷酸替代的合成条件

氧化环境中，铁氧化物的铁循环伴随着两个特点：(a) 不同原子价的铁氧化物存在；(b) 晶体结构中有多面体链的氧离子和氢氧离子（Waychunas, 1991）。Fe^{2+} 和 Fe^{3+}的移动性是通过电子跳跃产生的低活化能使 Fe^{2+} 变成 Fe^{3}来实现的，反之亦然。Waychunas（1991）揭示了铁氧化物的长程结构是通过不同结构矿物的组合（例如立方晶系的磁铁矿、针铁矿和六方晶系的赤铁矿）或者失去氧多面体链联合实现的。针铁矿沿[001]结晶方向每隔两个链丢失两个链。纤铁矿结构可以通过针铁矿结构丢失一个氧多面体而形成。至于磁铁矿和赤铁矿，他们之间没有链的丢失。通过这些多面体链以及铁离子电子跃迁造成的化学价变化，铁可以在除水铁矿以外的铁氧化物中循环。之所以排除水铁矿是因为水铁矿多面体链的晶体结构很差。

对于含氧量少和无氧条件下沉积物中的铁循环，电子的转移也十分重要。在

沉积环境中，有机质的降解会持续消耗 O_2, NO_3^- (有氧条件下), MnO_2, Fe_2O_3, FeOOH（低氧条件下）, SO_4^{2-}和 CO_2（无氧条件），这些都是电子的接受者，它们被利用的顺序和它们被还原后产生的自由能相反（Froelich et al., 1979）。有机质的降解一直持续到成岩作用初期，直到所有的有机质或氧化剂都被消耗。当有机质降解继续进行，尤其是到了次氧化阶段，岩石中的铁氧化物（和其他含铁矿物）通过硫化和黄铁矿化（形成黄铁矿）被逐步溶解（Canfield and Berner, 1987; Karlin and Levi, 1983, 1985; Karlin, 1990a, b; Channell and Hawthorne, 1990; Rowan et al., 2009）。不同的铁氧化物对硫化物有不同的反应程度，反应程度大小顺序如下：水合铁氧化物、纤铁矿、针铁矿、磁铁矿和赤铁矿[Poulton et al., 2004]。SO_4^{2-}还原产生可溶硫化物，可溶性硫化物（H_2S 和 HS^-）促进铁还原产生 Fe^{2+}的反应，导致自生作用铁的硫化物沉淀，包括亚铁胶黄铁矿（Roberts and Turner, 1993; Reynolds et al., 1994; 1999; Roberts et al., 2011a）。亚铁磁性单斜磁黄铁矿的形成经常被错误地认为是早期成岩作用生成黄铁矿的中间产物（cf. Sweeney and Kaplan, 1973）。Horng and Roberts（2006）则认为六棱形（hexagonal）磁黄铁矿（常温为反铁磁性）只能在成岩作用初期形成，而现代沉积物中只含有碎屑单斜磁黄铁矿，自生的单斜磁黄铁矿则在成岩作用后期形成，因而可以携带后期的磁化强度。在无氧无硫环境下，铁硫化物形成被抑制，当裂隙水中的 CO_2 饱和时将会形成菱铁矿。多余的 Fe^{2+}可以在沉积物中向上扩散直到遇到氧化或次氧化条件，然后再次以铁氧化物形式沉积（Karlin et al., 1987），或者被趋磁细菌生物矿化（e.g., Schüler and Baeuerlein, 1996; Tarduno and Wilkison, 1996; Flies et al., 2005; Roberts et al., 2011b）。另外，有机质可能绝大部分在埋藏之前就被降解，这是由于海床有机碳通量较低或（和）底层水氧气含量较高导致。这样的氧化条件将驱使自生铁氧化物形成，因此陆源沉积信息和自生信息同时被保存（e.g., Henshaw and Merrill, 1980）。

文献速递

1. 太平洋热带地区台风活动的增加受冰河时代环流变化的驱动

翻译人：仲义 zhongy@sustech.edu.cn

Bramante J F, Ford M R, Kench P S, et al. ***Increased typhoon activity in the Pacific deep tropics driven by Little Ice Age circulation changes*** *[J] Nature Geoscience, 2020, online.*

https://doi.org/10.1038/s41561-020-00656-2

摘要：气象设备监测记录显示热带气旋活动在年际和年代际尺度上对海洋和大气的变化很敏感。然而，我们基于气候对热带气旋行为影响的认识受到历史记录较短和史前重建记录稀少的限制，特别是在西北太平洋地区，那里沿海社区每年都会因台风而失去生命和工作。因此，本文作者为了过去区域性台风动态变化，重建了 3000 年来北太平洋热带气旋现象。结合现有的记录，我们的重建表明，1350 年以前的低基线台风活动以后，在小冰期伴随着风暴的频率增多。这一模式与水文气候变化同时出现，表明太平洋水文气候和热带气旋气候之间存在百年尺度的联系。一组全球气候模型证实小冰河期两种太平洋气候模式中存在太平洋沃克环流的迁移和变异，这可能有助于增强北太平洋热带西部的热带气旋活动。在下个世纪中，预计太平洋沃克环流的变化和热带的扩张将逆转的小冰期的水文气候趋势，有可能减少热带太平洋深处的台风活动。

ABSTRACT: The instrumental record reveals that tropical cyclone activity is sensitive to oceanic and atmospheric variability on inter-annual and decadal scales. However, our understanding of the influence of climate on tropical cyclone behaviour is restricted by the short historical record and the sparseness of prehistorical reconstructions, particularly in the western North Pacific, where coastal communities suffer loss of life and livelihood from typhoons annually. Here, to explore past regional typhoon dynamics, we reconstruct three millennia of deep tropical North Pacific cyclogenesis. Combined with existing records, our reconstruction demonstrates that low-baseline typhoon activity prior to 1350 ce was followed by an interval of frequent storms during the Little Ice Age. This pattern, concurrent with hydroclimate proxy variability, suggests a centennial-scale

link between Pacific hydroclimate and tropical cyclone climatology. An ensemble of global climate models demonstrates a migration of the Pacific Walker circulation and variability in two Pacific climate modes during the Little Ice Age, which probably contributed to enhanced tropical cyclone activity in the tropical western North Pacific. In the next century, projected changes to the Pacific Walker circulation and expansion of the tropics will invert these Little Ice Age hydroclimate trends, potentially reducing typhoon activity in the deep tropical Pacific.

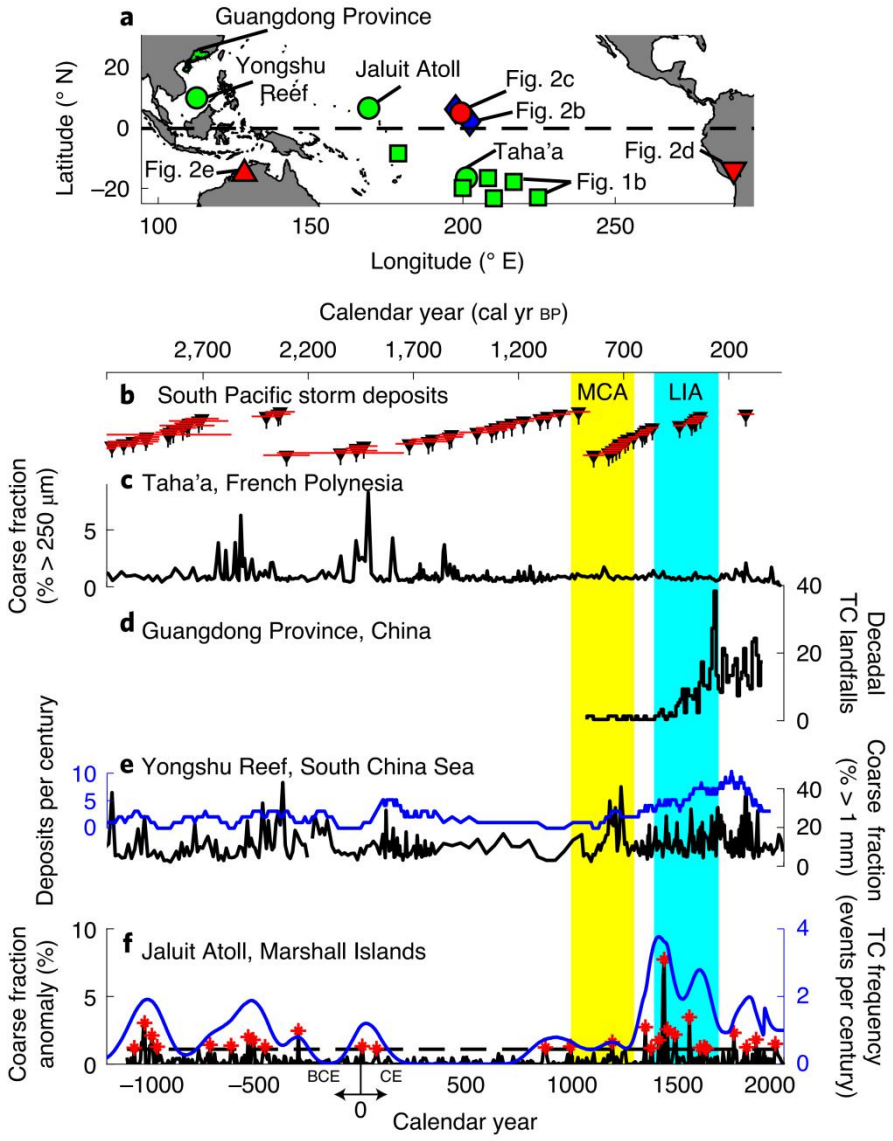

Figure 1. Western Pacific tropical cyclone reconstructions. a, Location of records in Figs. 1 and 2; symbol definitions can be found in Extended Data Fig. 1. b, Radiocarbon dates (±1 standard deviation) from South Pacific storm-deposited boulders[21,22]. c, Storm deposits in a back-barrier reef lagoon,

Taha'a, French Polynesia[20]. d, TC landfalls in Guangdong Province and imperial Chinese historical records[10]. e, Coarse fraction (black line) and centennial frequency (blue line) of large wave deposits at Yongshu Reef[11]. f, Coarse fraction (250–2,000 μm) anomaly (black line) from Jaluit Atoll and centennial frequency (blue line) of identified storm deposits (red asterisks) (this study). The error in c, e and f is less than ±0.05%, which is too small for plotting. Uncertainty estimates were unavailable for d.

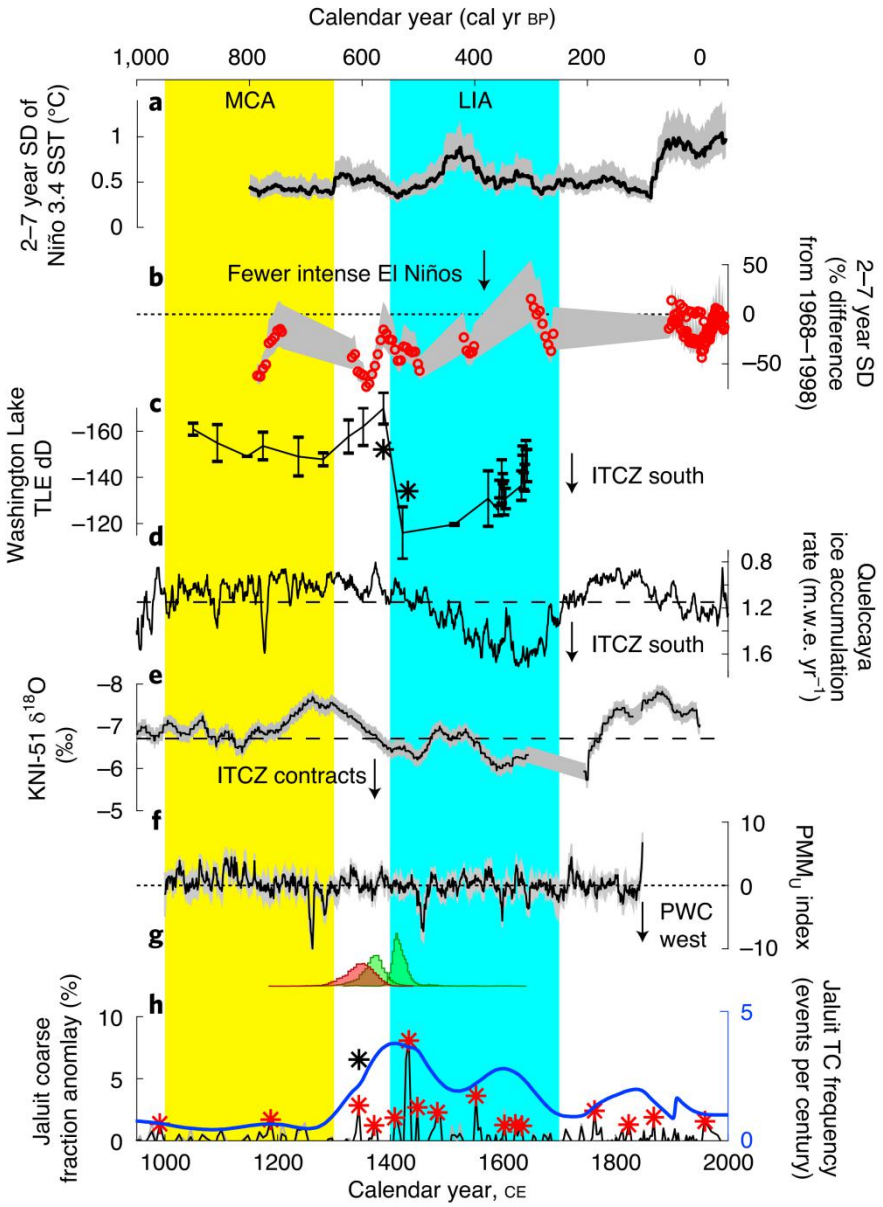

Figure 2. Comparison of our storm reconstruction with Pacific paleoclimate proxies. a, ENSO-band standard deviation (SD) calculated in a 31-year moving window of a multi-proxy reconstruction of Niño 3.4 region SST anomalies[26]. b, Normalized ENSO-band SD of SSTs from coral $\delta^{18}O$ proxies[28,50]. c, Lipid δD proxy of precipitation from Washington Lake, Washington Island, Northern Line Islands[32].

d, Ice accumulation rates in metres water equivalent (m.w.e.) in a core from the Quelccaya ice cap, Peru33. e, Speleothem $\delta^{18}O$ proxy of precipitation from cave KNI-51, northwestern Australia[29]. f, CMIP5 ensemble median (black line) ± standard error (grey shading) of decadally averaged PMM wind index anomaly (this study). g, Comparison of age model histograms from samples indicated by black asterisks in c and h. h, same as Fig. 1f. The dashed black lines indicate 1000–1850 ce means and the dotted black lines indicate zero values. The grey shading in a, b and e indicate 95% confidence intervals. Uncertainty estimates unavailable for d.

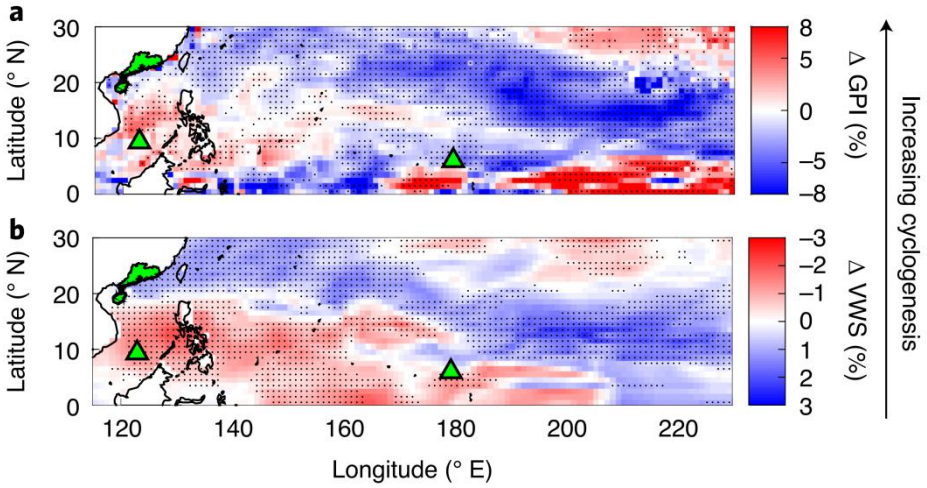

Figure 3. Change in tropical cyclogenesis potential from the MCA (1000–1300 ce) to the LIA (1400–1700 ce). a,b, Ensemble median relative anomaly (Δ = (LIA - MCA)/MCA × 100%) of (a) GPI and (b) VWS. Anomalies for all GPI components are plotted in Extended Data Fig. 5. Anomalies were calculated from Northern Hemisphere storm season (JASON) averages. The black stippling indicates that five of the seven models agree on change direction. The green symbols represent locations of storm reconstructions (Extended Data Fig. 1)

2. 南开海槽俯冲带温度对深部生命的限制

翻译人：蒋晓东 jiangxd@sustech.edu.cn

Heuer V B, Inageaki F, Morono, et al. ***Temperature limits to deep subseafloor life in the Nankai Trough subduction zone*** *[J]. Science, 2020, 370: 1230-1234.*

https://doi.org/10.1126/science.abd7934

摘要：深海深部沉积物中的微生物对全球生物量具有重要贡献。当沉积物中温度超过 40 度时，沉积物体积会迅速减半。在这样难以评估的环境中，微生物总量对这样的升温过程具有怎样的响应仍然不清楚。在南开海槽俯冲带中我们分析了深度达 1.2 km，温度达 120 度的沉积物中的微生物。当温度超过 45 度后植物细胞降低了 2 个数量级，内孢子总量上升到植物细胞的 6000 倍。沉积物温度达到 80-85 度时，作为生物学的产物-甲烷被氧化。在 100-120 度的沉积物中，同位素与细胞量的证据揭示超嗜热菌的存在。超过 45 度的微生物区交替到 192 m 的沉积物区并未检测到微生物。

ABSTRACT: Microorganisms in marine subsurface sediments substantially contribute to global biomass. Sediments warmer than 40 °C account for roughly half the marine sediment volume, but the processes mediated by microbial populations in these hard-to-access environments are poorly understood. We investigated microbial life in up to 1.2-kilometer-deep and up to 120 °C hot sediments in the Nankai Trough subduction zone. Above 45 °C, concentrations of vegetative cells drop two orders of magnitude and endospores become more than 6000 times more abundant than vegetative cells. Methane is biologically produced and oxidized until sediments reach 80 ° to 85 °C. In 100 ° to 120 °C sediments, isotopic evidence and increased cell concentrations demonstrate the activity of acetate-degrading hyperthermophiles. Above 45 °C, populated zones alternate with zones up to 192 meters thick where microbes were undetectable.

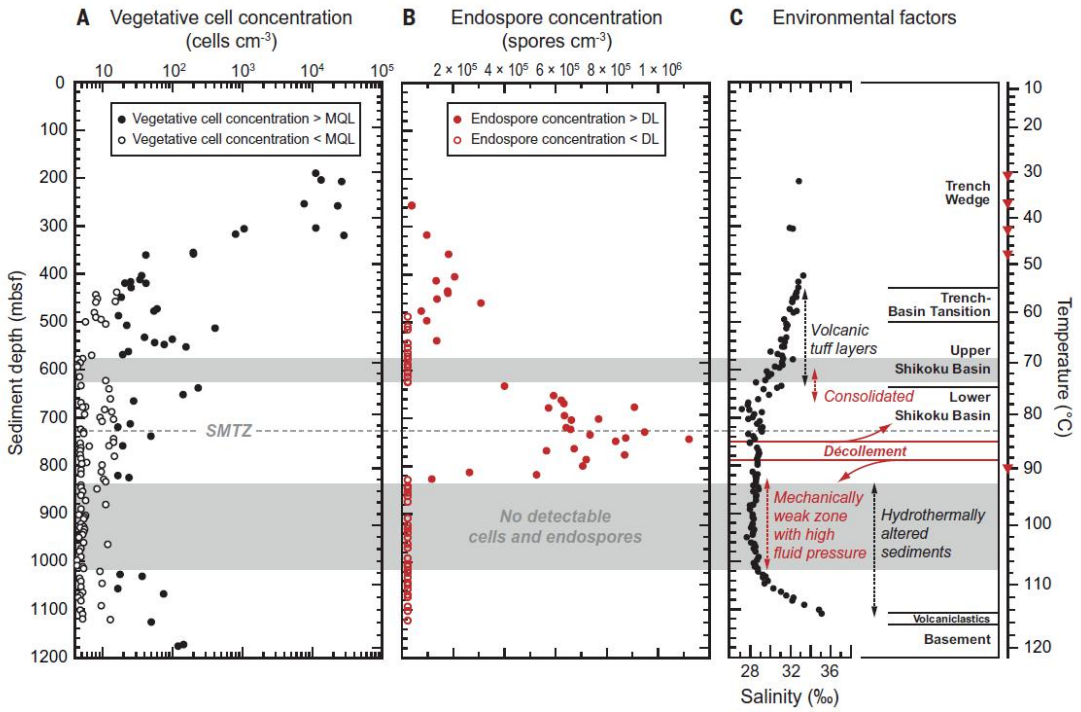

Figure 1. Depth profiles of vegetative cells and endospores in relation to environmental factors at IODP Site C0023. (A) Concentrations of vegetative cells determined by counting of microbial cells fluorescently stained with SYBR Green I. (B) Concentrations of bacterial endospores derived from analysis of the diagnostic biomarker DPA; analytical sensitivity corresponds to a detection limit (DL) of 2.2×10^4 endospores cm^{-3}. (C) A schematic summary of temperature, tectonic units, and salinity showing the geochemical influence of basalt alteration in the basement; red symbols on the temperature axis designate the depth horizons where in situ temperature measurements were made. Gray shading indicates zones where concentrations of both vegetative cells and endospores were undetectable in all samples; the gray dashed line indicates the location of the SMTZ.

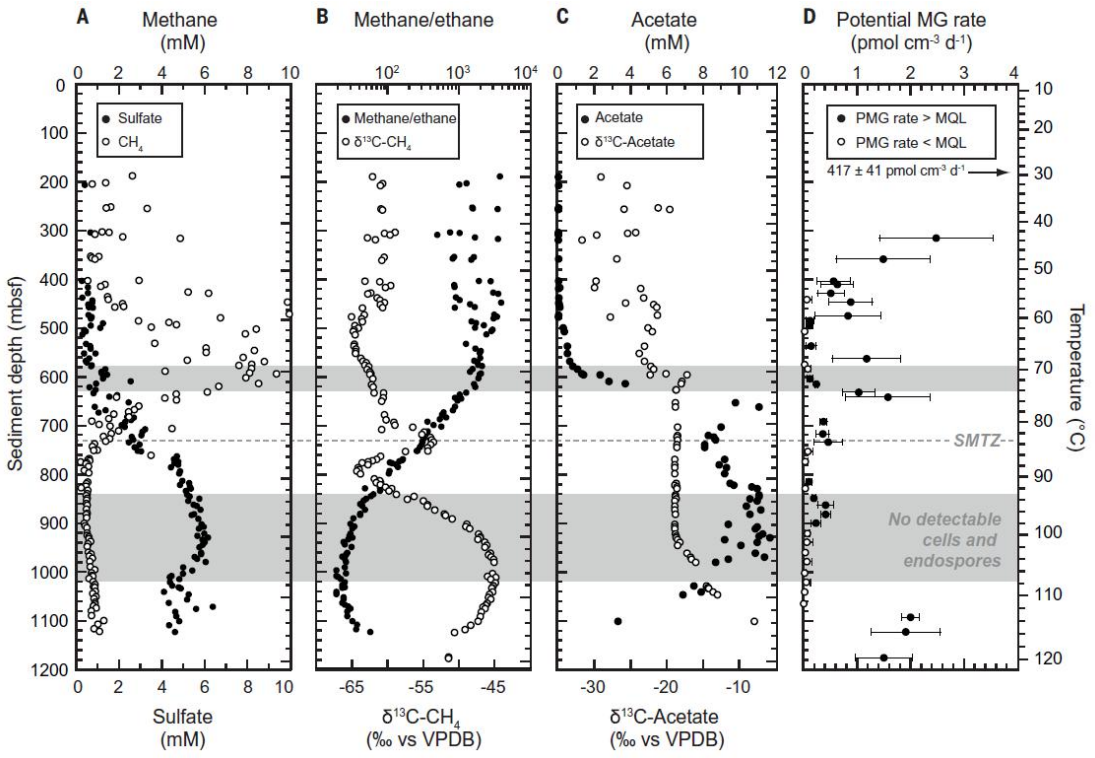

Figure 2. Geochemical signals of microbial metabolism at Site C0023. (A to D) (A) Dissolved methane (13) and sulfate (13), (B) methane/ethane ratios (13) and δ^{13}C-CH_4, (C) dissolved acetate and δ^{13}C-acetate, and (D) potential rates of methanogenesis (MG) based on conversion of ^{14}C-CO_2 to ^{14}C-CH_4; note that the value at 180 mbsf is off-scale. Potential MG (PMG) rates were determined at 40 °C for ≤ 360 mbsf, 60 °C for 405 to 585 mbsf, 80 °C for 604 to 775 mbsf, and 95 °C for ≥ 816 mbsf. The MQL was 0.094 pmol CH4 cm^{-3} day^{-1}. Gray shading, SMTZ, and the temperature axis are as in Fig. 1. VPDB in (B) and (D) is the Vienna Pee Dee Belemnite standard. In (D), error bars represent the standard deviation of three replicates.

3. 金红石中纳米级的微量元素团簇的地球化学和年代学意义

翻译人：冯婉仪 fengwy@sustech.edu.cn

Verberne R, Reddy S M, Saxey D W, et al. ***The geochemical and geochronological implications of nanoscale trace-element clusters in rutile*** *[J]. Geology, 2020, 48: 1126-1130. https://doi.org/10.1130/G48017.1*

摘要：金红石中微量元素的地球化学分析（如：Pb、U 和 Zr）通常用于提取有关地质事件的性质和时间的信息。然而，微量元素的迁移性可以影响温度和年龄的测定，而控制迁移性的机制仍然存在争议。为了进一步探讨这一问题，我们使用 LA-ICPMS 和原子探针断层扫描来表征来自澳大利亚西部 Capricorn 造山带的金红石中微量元素在微米-纳米尺度上的分布。在大于 20 μm 的尺度上，单颗粒中没有显著的微量元素变化，并且 1872 ± 6 Ma (2σ) 的 U-Pb 谐和年龄显示没有同位素干扰的证据。在纳米尺度上，可以观察到高达 20 nm 大小的团簇，并且这些团簇富集微量元素（Al、Cr、Pb 和 V）。团簇的 $^{207}Pb/^{206}Pb$ 比值为 0.176 ± 0.040（2σ），表明它们形成于结晶之后，可能是在区域变质过程中形成的。我们认为该团簇是由高角闪岩相变质过程中放射性破坏的瞬态位置捕获迁移的微量元素而形成的。捕获会影响团簇内元素体积扩散的活化能。少量和低密度的团簇提供了约束团簇的形成时间，表明变质温度峰值是短暂的、小于 10 m.y.的事件。我们的结果表明，用微量元素估计金红石的体积扩散比假设其为均匀介质更为复杂。

ABSTRACT: The geochemical analysis of trace elements in rutile (e.g., Pb, U, and Zr) is routinely used to extract information on the nature and timing of geological events. However, the mobility of trace elements can affect age and temperature determinations, with the controlling mechanisms for mobility still debated. To further this debate, we use laser-ablation–inductively coupled plasma–mass spectrometry and atom probe tomography to characterize the micro- to nanoscale distribution of trace elements in rutile sourced from the Capricorn orogen, Western Australia. At the >20 μm scale, there is no significant trace-element variation in single grains, and a concordant U-Pb crystallization age of 1872 ± 6 Ma (2σ) shows no evidence of isotopic

disturbance. At the nanoscale, clusters as much as 20 nm in size and enriched in trace elements (Al, Cr, Pb, and V) are observed. The $^{207}Pb/^{206}Pb$ ratio of 0.176 ± 0.040 (2σ) obtained from clusters indicates that they formed after crystallization, potentially during regional metamorphism. We interpret the clusters to have formed by the entrapment of mobile trace elements in transient sites of radiation damage during upper amphibolite facies metamorphism. The entrapment would affect the activation energy for volume diffusion of elements present in the cluster. The low number and density of clusters provides constraints on the time over which clusters formed, indicating that peak metamorphic temperatures are shortlived, <10 m.y. events. Our results indicate that the use of trace elements to estimate volume diffusion in rutile is more complex than assuming a homogeneous medium.

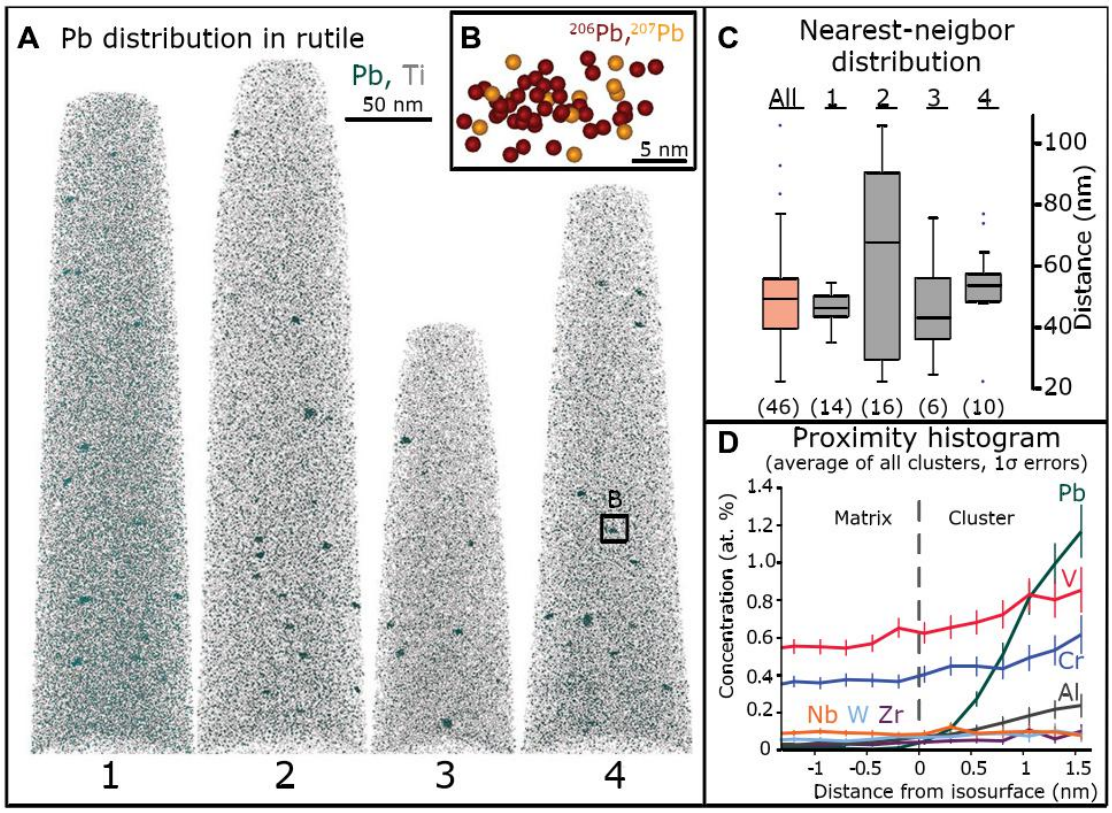

Figure 1. (A) Images of four atom probe tomography reconstructions showing Pb clusters (see Video S1 [footnote 1]). (B) Close-up image of one of the Pb clusters from specimen 4, showing distribution of ^{206}Pb and ^{207}Pb. (C) Box plots showing nearest-neighbor distribution of individual specimens and combined values (red); number of clusters is given in parentheses. Box—interquartile range; horizontal lines—minimum and maximum value of each quartile; horizontal line inside box—median;

dots—potential outliers. (D) Proximity histogram based upon all 46 Pb clusters, showing profile of Pb, Al, Cr, Nb, V, W, and Zr; error bars are 1σ.

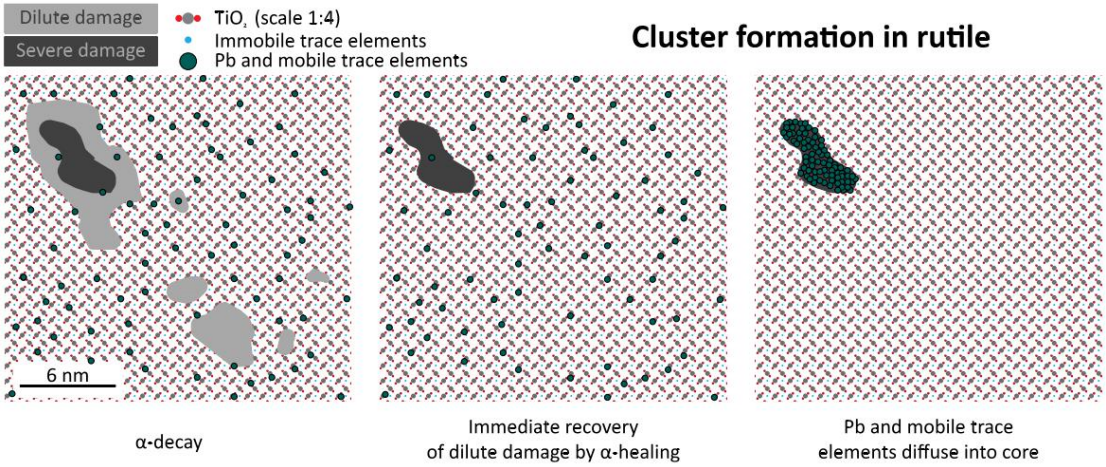

Figure 2. Schematic model for formation of Pb clusters in rutile based on radiation-damage experiments (Trachenko et al., 2006). (A) α-decay creates two radiation damage zones: dilute and severe. (B) Dilute damage recovers instantly due to α-healing. (C) Within a limited temperature window, Pb can migrate over short distances in a severely damaged zone. If temperatures are too low, there would be no migration and damage would recover over time. If temperatures are higher, Pb loss might occur and damage recovery would be faster.

4. FORC 图的主成分分析方法区分太平洋红层中的生物成因和陆源磁性矿物的组分以及古环境的指示意义

翻译人：李园洁 liyj3@sustech.edu.cn

Yamazaki T, Fu W, Shimono T, et al. ***Unmixing biogenic and terrigenous magnetic mineral components in red clay of the Pacific Ocean using principal component analyses of first-order reversal curve diagrams and paleoenvironmental implications*** *[J]. Journal of Geophysical Research: Solid Earth, 2020, 72: 120.*

https://doi.org/10.1186/s40623-020-01248-5

摘要：红色粘土广泛分布在中纬度远洋环境的海底，保存着长尺度的古海洋记录。本文作者对太平洋红层进行岩石磁学的研究来解释古环境的变化。样品来自南太平洋的 IODP 的 U1365A 孔的岩芯和北太平洋西部的三个活塞岩芯。对一阶反转曲线图进行主成分分析（FORC-PCA）揭示出北太平洋西部的岩芯有三个磁组分（端元 EM1 到 EM3）。EM1 表示相互作用单畴和涡旋的特征，可解释为陆源。EM2 和 EM3 具有不同矫顽力分布的无相互作用的 SD 颗粒，可解释为生物来源。在~ 2.7 m 深度 EM1 分布突然增加，表明风尘输入增加。这个时间的年龄大约在始新世-渐新世（E/O）分界。透射电子显微镜显示 EM2 主要是等八面体形态的磁小体，而 EM3 具有更多的子弹形态的磁小体。在~ 6.7-8.2 m 深度 EM3 的增加表明沉积物处于有氧-缺氧过渡带（OATZ）。OATZ 的化学条件是由赤道附近的更高的生物生产力造成的。对 U1365A 孔的岩芯的 FORC-PCA 揭示出两个 EM 组分，陆源（EM1）和生物成因（EM1）。U1365A 孔生物成因组分的矫顽力分布与北太平洋西部的低矫顽力生物成因组分的类似。在 E/O 分界处 U1365A 孔的陆源组分也明显突然增加。这种陆源组分的增加可能是由亚洲和澳大利亚干旱区域背风处缓慢构造漂移造成的。另外，风尘增加在两个半球是同时期的，可能与 E/O 分界时全球变冷有关。

ABSTRACT：Red clay widely occupies the seafloor of pelagic environments in middle latitudes, and potentially preserves long paleoceanographic records. We conducted a rock-magnetic study of Pacific Ocean red clay to elucidate paleoenvironmental changes. Three piston cores from the western North Pacific Ocean and IODP Hole U1365A cores in the South Pacific Ocean were

studied here. Principal component analyses applied to first-order reversal curve diagrams (FORC-PCA) reveals three magnetic components (endmembers EM1 through EM3) in a core of the western North Pacific. EM1, which represents the features of interacting single-domain (SD) and vortex states, is interpreted to be of terrigenous origin. EM2 and EM3 are carried by non-interacting SD grains with different coercivity distributions, which are interpreted to be of biogenic origin. The EM1 contribution suddenly increases upcore at a depth of ~ 2.7 m, which indicates increased eolian dust input. The age of this event is estimated to be around the Eocene – Oligocene (E/O) boundary. Transmission electron microscopy reveals that EM2 is dominated by magnetofossils with equant octahedral morphology, while EM3 has a higher proportion of bullet-shaped magnetofossils. An increased EM3 contribution from ~ 6.7 to 8.2 m suggests that the sediments were in the oxic-anoxic transition zone (OATZ), although the core is oxidized in its entire depth now. The chemical conditions of OATZ may have been caused by higher biogenic productivity near the equator. FORC-PCA of Hole U1365A cores identified two EMs, terrigenous (EM1) and biogenic (EM2). The coercivity distribution of the biogenic component at Hole U1365A is similar to that of the lower coercivity biogenic component in the western North Pacific. A sudden upcore terrigenous-component increase is also evident at Hole U1365A with an estimated age around the E/O boundary. The increased terrigenous component may have been caused by the gradual tectonic drift of the sites on the lee of arid continental regions in Asia and Australia, respectively. Alternatively, the eolian increase may have been coeval in the both hemispheres and associated with the global cooling at the E/O boundary.

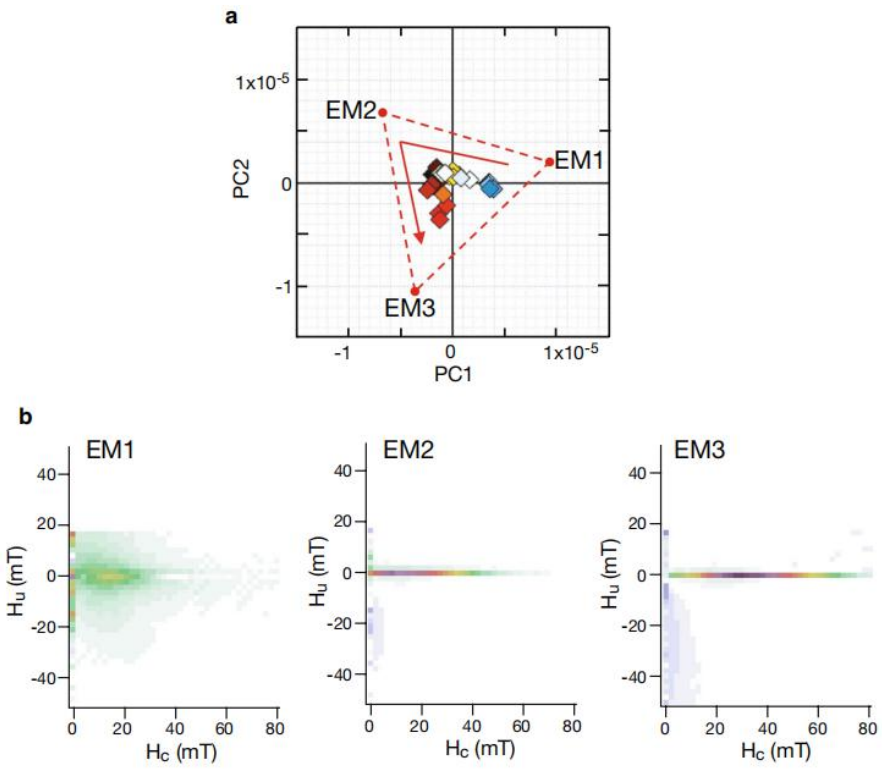

Figure 1. Principal component analysis (PCA) of frst-order reversal curve (FORC) diagrams for core KR13-02 PC06. a Distribution of 26 FORC data (squares) on the principal component PC1-PC2 plane. Triangular dashed lines defne a three-endmember (EM) system, and the arrow indicates the general downcore trend. b FORC diagrams for EM1, EM2, and EM3

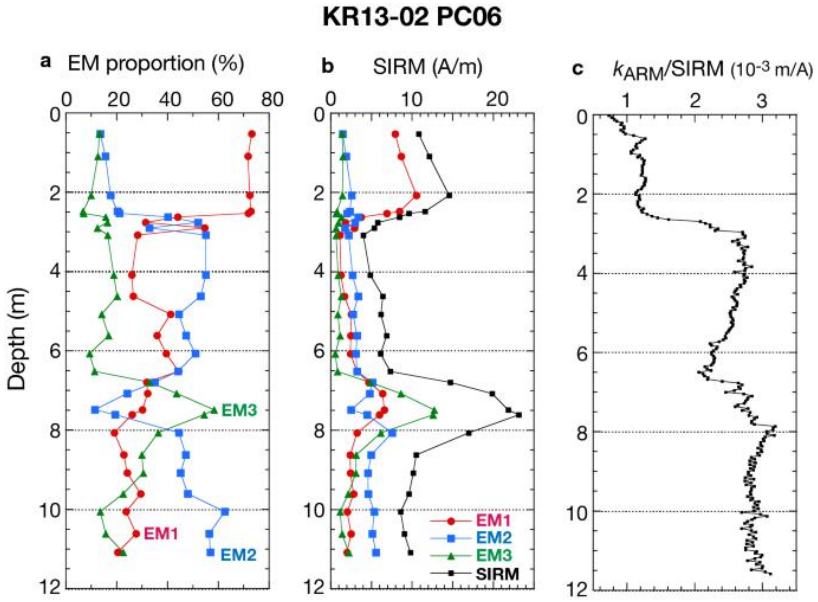

Figure 2. Downcore variations of FORC-PCA endmembers (EMs) and k_{ARM}/SIRM for core KR13-02 PC06. a The proportion of EM1 (red), EM2 (blue), and EM3 (green). b SIRM (black) and the contribution to SIRM of individual EMs calculated from the respective proportions. c Variations of

k_{ARM}/SIRM. Note the synchronous changes of EMs and k_{ARM}/SIRM at~2.7 m, and an EM3 increase between~6.7 and 8.2 m.

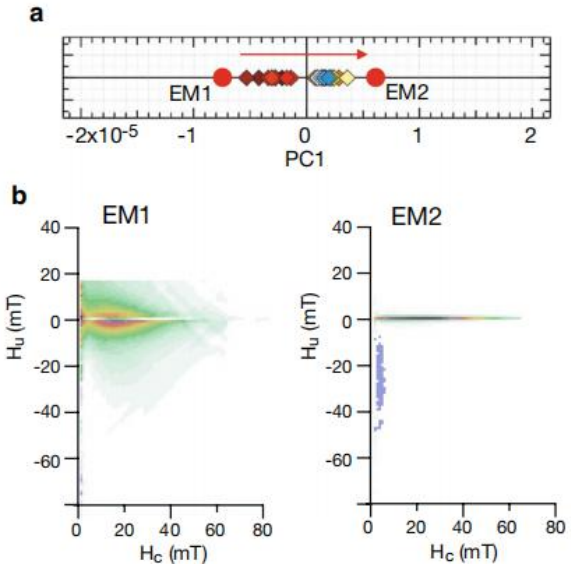

Figure 3. FORC-PCA results for samples from IODP Hole U1365A, South Pacifc Ocean. a Distribution of 30 FORC data (squares) in PC1 space with two-endmembers (EM1 and EM2). The arrow indicates the general downcore trend. b FORC diagrams for EM1 and EM2.

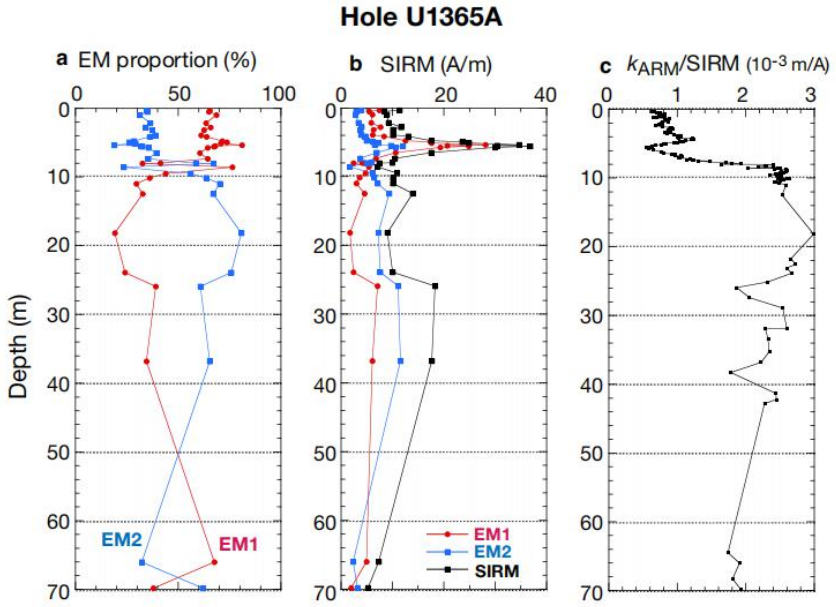

Figure 4. Downcore variations of FORC-PCA EMs and k_{ARM}/SIRM for Hole U1365A. a Proportions of EM1 (red) and EM2 (blue). b SIRM (black) and the contribution of individual EMs calculated from the respective proportions. c Variations of k_{ARM}/SIRM (Shimono and Yamazaki, 2016). Note the synchronous EM and k_{ARM}/SIRM changes at~8 m in depth.

5. 对西非过去 0-2000 AD 地磁场变化的新见解—基于新的 0-2000 AD 古强度曲线

翻译人：柳加波 Liujb@sustech.edu.cn

Kapper L, Serneels V, Panovska S, et al. ***Novel insights on the geomagnetic field in West Africa from a new intensity reference curve (0-2000 AD)*** *[J]. Scientific reports, 2020, 10(1): 1-15. https://doi.org/10.1038/s41598-020-57611-9*

摘要：过去两千年中非洲地磁场的变化仍然存在很大未知。尽管考古文物能够可靠得记录古代地磁场强度，但迄今鲜有来自非洲的考古古强度数据。本文，我们使用 Thellier-Coe 方法和经过校准的伪 Thellier 方法，从年代久远的考古文物中建立来自布基纳法索和科特迪瓦（西非）的古地磁场强度。通过将 18 个新数据与之前已发表的西非古强度数据整合，我们重建了过去 2000 年西非古地磁场强度参考曲线。为了获得可靠的古强度参考曲线，我们结合了 bootstrap 自举法，评估了一种正则（惩罚回归）平滑样条拟合和一种随机建模方法。两条强度曲线都有很好的吻合，支持我们提出的 0-2000 AD 古强度变化置信度。此外，由于数据处理和不确定性方法的不同，两条强度曲线仅产生细微差异。在大约公元 740 年和公元 1050 两个主峰，在我们和其他位置的参考曲线中似乎都是常见的，这指示了一个相当稳定的地磁场特征，即从中国到夏威夷西向运动。然而，在不同位置不相关的独立小峰可能暗示了地磁场的局部表达，可能是非偶极子场的变化。

ABSTRACT: The geomagnetic field variations on the continent of Africa are still largely undeciphered for the past two millennia. In spite of archaeological artefacts being reliable recorders of the ancient geomagnetic field strength, only few data have been reported for this continent so far. Here we use the Thellier-Coe and calibrated pseudo-Thellier methods to recover archaeointensity data from Burkina Faso and Ivory Coast (West Africa) from well-dated archaeological artefacts. By combining our 18 new data with previously published data from West Africa, we construct a reference curve for West Africa for the past 2000 years. To obtain a reliable curve of the archaeointensity variation, we evaluate a penalized smoothing spline fit and a stochastic modelling method, both combined with a bootstrap approach. Both intensity curves

agree well, supporting the confidence in our proposed intensity variation during this time span, and small differences arise from the different methodologies of treating data and uncertainties. Two prominent peaks at around 740 AD and 1050 AD appear to be common in ours and several reference curves from other locations, indicating a general westward movement from China to Hawaii of a rather stable feature of the geomagnetic field. However, independent smaller peaks that do not correlate in different locations may hint to localized expressions of the geomagnetic field as a result of temporarily varying non-dipole sources.

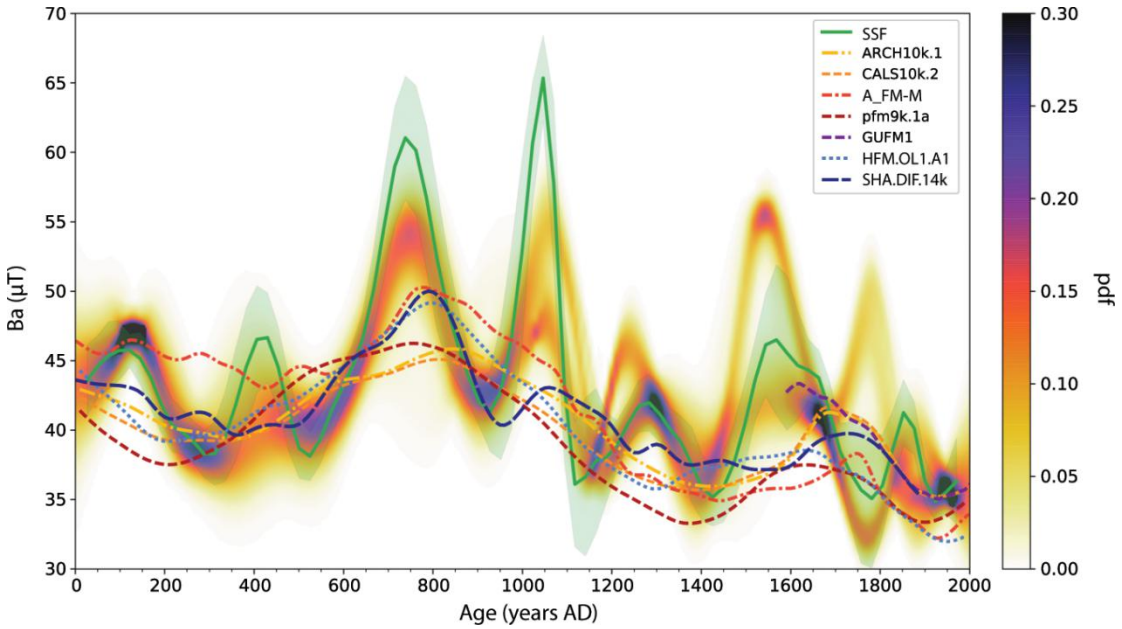

Figure 1. Comparison of West African curves - smoothing spline fit (SSF) and stochastic modelling curve as probability density function (pdf) - with the following global geomagnetic field models: ARCH10k.1, CALS10k.2, A_FM-M, pfm9k.1a, GUFM1, HFM.OL1.A1, SHA.DIF.14k.

6. 南海神狐区域细粒沉积物粒度特征及其与天然气水合物饱和度的关系

翻译人：刘伟 inewway@163.com

Su M, Luo K, Fang Y, et al., ***Grain-size characteristics of fine-grained sediments and association with gas hydrate saturation in Shenhu Area, northern South China Sea*** *[J]. Ore Geology Reviews, 2020, online.*

https://doi.org/10.1016/j.oregeorev.2020.103889

摘要：天然气水合物储层是世界范围内的研究热点，其中神狐地区（位于南海北坡）是世界级的天然气水合物勘探区。然而，细粒度天然气水合物储层的岩性、物性和物源并不为人所知。研究沉积粒度参数如何影响细粒度的天然气水合物储层质量，可以为储层评价提供重要的突破口。广州海洋地质调查局从各次考察中收获的 8 个岩芯，与 2D/3D 地震数据相结合，为系统研究天然气水合物储层与周围沉积物的粒径参数特征提供了难得的机会。

结合岩性、粒大小特征（平均粒度、分选度、偏度、峰度）、高分辨率地震特征以及相关的双变量和聚类分析结果，可识别两个沉积层段为两种不同沉积过程。下部沉积段的粗粒径含量比上部层段要高，其层位与天然气水合物富集非常一致。而上部层段则不富集天然气水合物。关于井 G 中未固结的天然气水合物储层沉积物，孔隙度（52%～64%）和分选系数（1.68～2.2）变化有限，高天然气水合物饱和度（> 30%）发生在顶层。天然气水合物饱和度与粗粒径（1%粗粒度）之间的正相关（R = 0.55）表明，粗粒组分的增加有利于孔喉的扩大，并改善初始渗透性和储层特性。

1%粗粒度和中值粒径的地震特征和相关图表明，下部薄层富水合物的细粒沉积物可能是浊积复合体，包括水道/堤坝/朵叶和块体沉积。如果是这样的话，那么可以推断出浊积物具有良好的储层物理特性，有利于天然气水合物的形成和聚集。对第四纪细粒浊积物与天然气水合物饱和度关系的认识，可能有助于更清楚地了解包括南海神弧地区在内的全球细粒度天然气水合物储层的特点。

ABSTRACT: Fine-grained gas hydrate (GH) reservoirs are extensively studied worldwide, among which the Shenhu Area (located on the northern slope of the South China Sea) is a

world-class GH exploration area. However, the lithology, physical properties, and depositional origins of the fine-grained GH reservoirs are not well known. Understanding how sediment grain-size parameters affect the fine-grained GH reservoir quality could provide and important breakthrough for reservoir evaluation. Eight cores, recovered from various expeditions of the Guangzhou Marine Geological Survey, can be combined with 2D/3D seismic data to provide a rare opportunity to systematically investigate the grain-size characteristics of the GH reservoir, as well as the surrounding sediments.

A combination of lithology, grain size characteristics (mean size, sorting, skewness, kurtosis), high-resolution seismic features, and associated bivariate and cluster analysis results support the identification of two distinct intervals of fine-grained sediments that were deposited by different sedimentary processes. There is a relatively higher content of coarser silt in the lower interval than in the upper interval, and their boundary depths are highly consistent with those of the GH-bearing layer and the overlying non-GH-bearing layer. With respect to the unconsolidated GH-bearing sediments from Well G, both the porosity (52%–64%) and sorting coefficient (1.68–2.2) have limited variation, while high GH saturation (>30%) occurs at the top layer. The positive correlation between saturation and the coarsest one-percentile grain size (R=0.55) reveals that an increase in the coarse fraction/particle size favours the development of a larger pore throat diameter and improves the initial permeability and reservoir properties.

The seismic features and cross-plots of the coarsest one-percentile and median values indicate that the lower thin-bedded fine-grained sediments with hydrate may be fine-grained turbidite complexes, including channels/levees/lobes and mass transport deposits. If this is the case, then it may be inferred that turbidite sediments provide good reservoir physical properties, favourable for GH formation and accumulation. These insights into the relationship between the Quaternary fine-grained turbidites and GH saturation may promote a clearer understanding of the characteristics and development of fine-grained GH reservoirs globally, including in the Shenhu Area of the South China Sea.

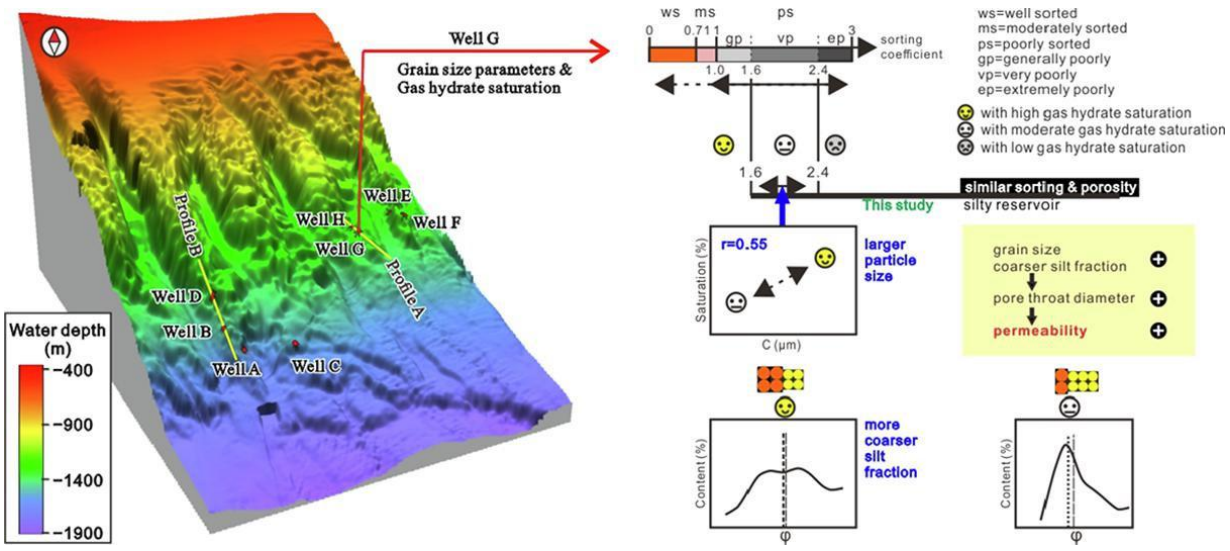

Figure 1. Graphical abstract

7. 磁测定位青铜时代晚期的畜栏

翻译人：曹伟 11930854@QQ.com

Smekalova T, Bevan B, Kashuba M, et al. ***Magnetic surveys locate Late Bronze Age corrals*** *[J]. Archaeological Prospection. 2020, online.*

https://doi.org/10.1002/arp.178914

摘要：在青铜时代晚期发现了一种新型的牲畜圈地。石墙勾勒出一对圆形或椭圆形区域，直径可达 50 米。石墙在地表是看不见的，它们是在克里米亚西北部通过遥感和地球物理调查的帮助发现的。在 2007 年到 2020 年间，超过 24 个这样的结构被发现；此前它们都没有被注意到。这些遗址的位置最初是在卫星图像中被发现的，通常是有异常绿色植被的地区。然后，大面积的磁测划定了埋藏的石头围护结构，因为非磁性石灰岩墙与磁性较强的土壤之间有很好的对比。特征扫描可以通过围墙的独特图案来识别：一个几乎完整的圆弧与一个完整的圆或椭圆形相连。土壤内的特征具有高水平的脲酶活性和高浓度的嗜热微生物。这意味着用动物粪便和植物残留物堆肥；因此，这些都是畜栏，饲养牲畜是当时经济的一部分。在大多数定居点中，只有一个双层围栏被发现；牲畜可能是所有居民所有的。每一个定居点都有几座住宅，并且都有土盆，其边缘用垂直的石板砌成。几个小面积的挖掘暴露了畜栏的墙壁。土壤和岩石的磁测量是建立磁模型的基础，计算的异常与磁图的测量结果一致。

ABSTRACT: A new type of livestock enclosure from the Late Bronze Age has been discovered. Stone walls outline a pair of circular or oval areas that may be up to 50 m in diameter. The stone walls are invisible at the surface; they were discovered in north-western Crimea and only with the aid of remote sensing and geophysical surveys. In the period 2007–2020, over two dozen of these structures were found; none has ever been noted before. The locations of these sites were first suggested in satellite imagery, often as areas with unusually green vegetation. Then, large-area magnetic surveys delineated the buried stone enclosures, for there was a good contrast between the non-magnetic limestone walls and the rather magnetic soil. The feature scan be identified by the unique pattern of the walls: An almost-complete circular arc that is connected to a full circle or

oval. The soil within the features has a high level of urease enzyme activity and a high concentration of thermophilic microorganisms. This suggests the composting of animal dung and plant residues; therefore, these were corrals and the raising of livestock was a part of the economy. Only one of the doubled enclosures is found at most settlements; the livestock were probably owned by all of the inhabitants. Each settlement had several dwellings, and these had earthen basins whose edges were lined with vertical stone slabs. Several small-area excavations exposed corral walls. Magnetic measurements of the soil and rock were the basis for magnetic models; the calculated anomalies agree with the measurements of the magnetic maps.

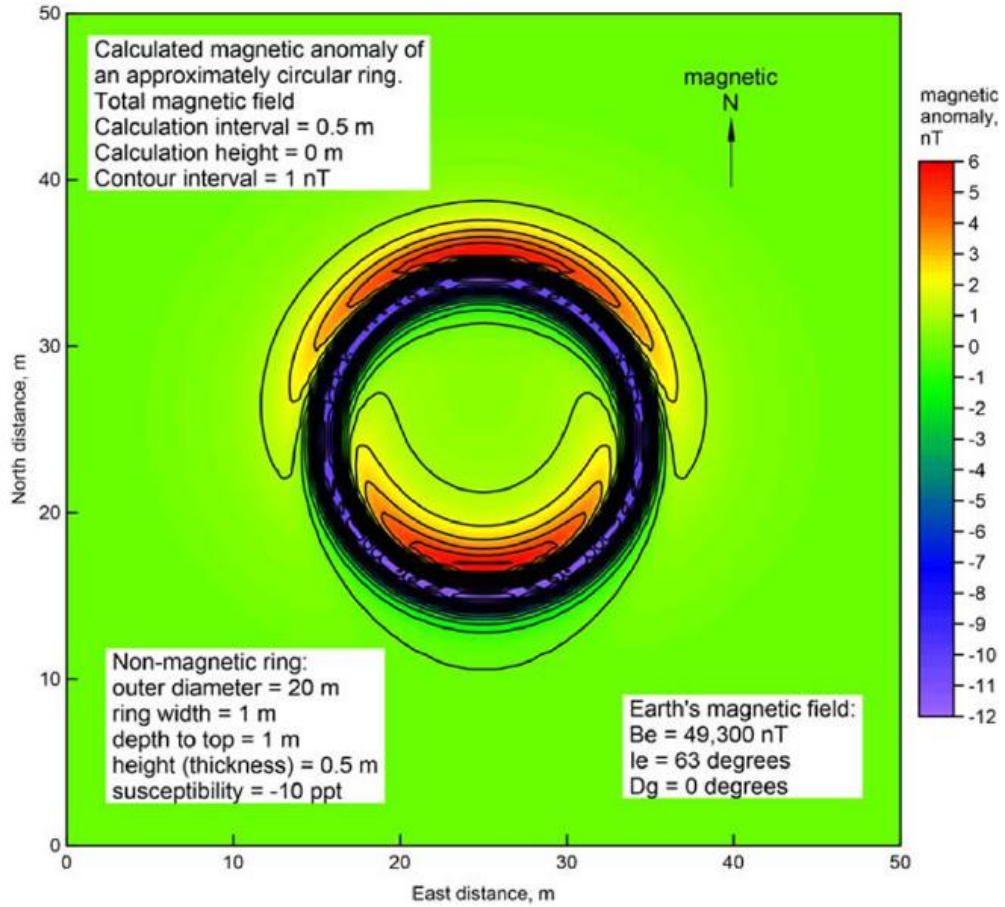

Figure 1. The magnetic anomaly of a circular ring. This calculated magnetic map approximates the anomaly of a stone circle. The magnetic low above the ring changes little around the circumference. However, the magnetic high to the north of the ring changes around the circumference; it is lowest on the east and west sides of the ring.

8. 青藏高原是如何动态影响夏季季风降水的?

翻译人：杨会会 11849590@mail.sustech.edu.cn

Son J H, Seo K H, Wang B. ***How does the Tibetan Plateau dynamically affect downstream monsoon precipitation?****[J].Geophysical Research Letters, 2020: 2020GL090543.*
https://doi.org/10.1029/2020GL090543

摘要：最近的研究表明，机械效应对东亚夏季风（EASM）的影响要大于热力效应。然而，其潜在动力机制的理论基础尚未阐明。之前的研究表明，地形强迫正压 Rossby 波理论很好地解释了季风降水的季节演变及其幅度和峰值位置。侵袭西藏的副热带纬向风高原是一个关键因素，由此产生的下游气旋性环流异常和反气旋性环流异常在两者之间形成一个纬向位势高度梯度峰值，导致经向风的发展，并伴随水汽输送到东亚季风区。随着季节接近夏季季风期，峰顶位势高度梯度—即季风雨带—从西北太平洋向西转移到东亚。本研究成果可应用于全球亚热带季风。

ABSTRACT: Recent studies have demonstrated that mechanical effects have a greater contribution to the East Asian summer monsoon (EASM) than thermodynamical effects. However, a theoretical basis for the underlying dynamical mechanism has not been elucidated. The present study shows that topographically forced barotropic Rossby wave theory well explains the seasonal evolution of the monsoonal precipitation and its amplitude and peak location. The subtropical zonal wind impinging on the Tibetan Plateau is a key factor, and the resulting downstream cyclonic and anticyclonic circulation anomalies form a peak zonal geopotential height gradient in between, leading to the development of the meridional wind and the accompanying moisture transport to the EASM region. As the season approaches the summer monsoon period, the peak geopotential height gradient – thus the monsoonal rainband – shifts to the west from the western North Pacific to East Asia. The findings in this study can be applied to subtropical monsoons worldwide.

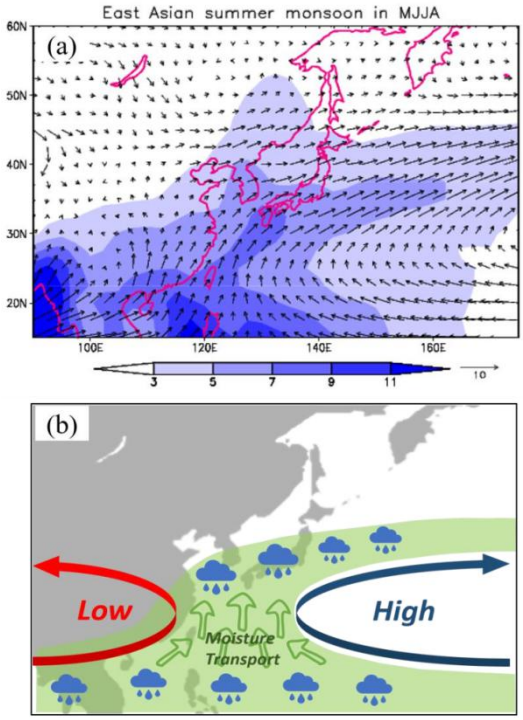

Figure 1. Characteristics of the East Asian summer monsoon (EASM). (a) Climatological mean precipitation and horizontal wind at 850 hPa in boreal summer (May to August), and (b) schematic of the EASM.

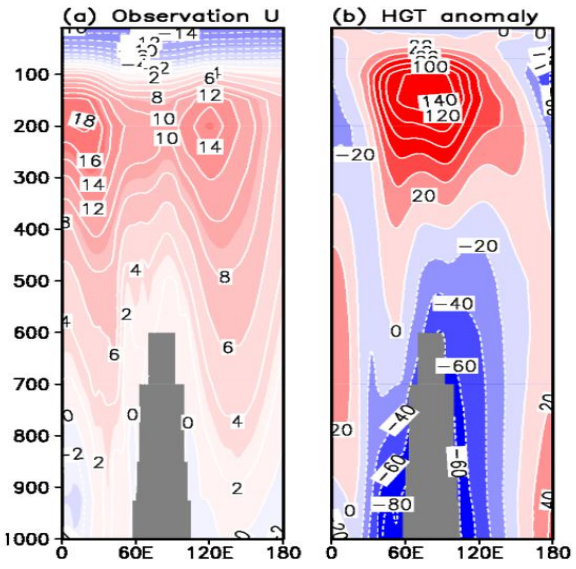

Figure 2. Vertical structure of the atmosphere around the Tibetan Plateau. Vertical and zonal cross-section of (a) zonal wind (m s^{-1}) and (b) geopotential height (m), averaged over 25°–35°N during May–August. The geopotential height anomaly is calculated by deviations from the zonal average at each pressure level.

9. 洞穴沉积物序列中人为产生的灰分层的磁性结构和古地磁分析（Crvena Stijena site, Montenegro）

翻译人：王浩森 11930841@mail.sustech.edu.cn

Bradák B, Carrancho Á, Herrejón lagunilla Á, et al. ***Magnetic fabric and archaeomagnetic analyses of anthropogenic ash horizons in a cave sediment succession (Crvena Stijena site, Montenegro)*** *[J]. Geophysical Journal International, 2020 , 224: 795-812.*

https://doi.org/10.1093/gji/ggaa461

摘要：在 Montenegro Crvena Stijena 的岩石中，对处于旧石器时代中期沉积层 XXIV 的七个人为灰烬层上进行了古地磁学，岩石磁学和磁组构的研究。这项研究有多个目标，包括识别燃烧过程中形成的含铁矿物，评估这些燃烧特征是否适合记录地球磁场方向，磁组构的含义以及研究洞穴（岩石）中烧毁的物质，和确定燃烧后的蚀变过程。磁铁矿已被确定为灰分的主要铁磁成分。烟灰层表现出了较高的热磁可逆性，与其下面烧成黑色层的不可逆行为相反，后者与获得的不同温度有关。在得到了七个具有可接受统计意义上的的平均古地磁方向后发现，这些结果表明这些特征记录下了燃烧时的磁场方向。但是，其中一些超出了中纬度地区长期变化的预期范围，表明燃烧后发生了变化。灰分的磁组构的特征在于低场磁化率测量的各向异性。对基本各向异性参数（例如磁面理，磁线理，各向异性程度和形状参数）的统计分析（箱形图和箱线图），以及对立体图的主要磁化率的比较，揭示了不同灰分单元之间的变化。这些单元的水平和垂直取向的磁组构由扁平，扁长，呈线状组成，可能表明不同的侵蚀过程，例如重力定向，溶蚀作用，径流水，地下水的垂直迁移等。落石冲击对磁组构的燃烧/沉积后改变。总而言之，灰烬层的磁性特征显示了以前未在现场发现的燃烧后变化过程的发生。史前燃烧特征的变化过程通常是从宏观观察中识别出来的，但我们的研究表明，多个过程会影响它们，并且通常不会引起注意，因为它们是在微观尺度上发生的。准确识别该过程对于正确地对地点进行时间和文化解释至关重要（例如，收集定年样本，遗骸的地层位移）。因此，磁性方法是在旧石器时代研究中用于识别和评估影响史前火灾的过程的强大而有效的工具。

ABSTRACT: An archaeomagnetic, rock magnetic and magnetic fabric study has been carried out

on seven anthropogenic ash horizons in the Middle Palaeolithic sedimentary level XXIV at the rock shelter of Crvena Stijena ('Red Rock'), Montenegro. The study has multiple goals, including the identification of iron bearing minerals formed during combustion, assessment of the suitability of these combustion features for recording the Earth´s magnetic field direction, revelation of the magnetic fabric and its significance in the characterization of cave (rock shelter) burnt facies, and identification of post-burning alteration processes. Magnetite has been identified as the main ferromagnetic component of the ash. The ash layers exhibit a high thermomagnetic reversibility in contrast to the irreversible behaviour of their subjacent burnt black layers which is related to the different temperatures attained. Seven mean archaeomagnetic directions were obtained with acceptable statistical values indicating that these features recorded the field direction at the time of burning. However, some of them are out of the expected range of secular variation for mid-latitude regions suggesting post-burning alterations. The magnetic fabric of the ash was characterized by anisotropy of low field magnetic susceptibility measurements. Statistical analysis (box and whisker plot) of the basic anisotropy parameters, such as foliation, lineation, degree of anisotropy and the shape parameter, along with the alignment of the principal susceptibilities on stereoplots, revealed variation among the ash units. The diverse, oblate to prolate, lineated or strongly foliated, quasi-horizontally and vertically oriented fabrics of the units may indicate different slope processes, such as orientation by gravity, solifluction, run-off water, quasi-vertical migration of groundwater and post-burning/post-depositional alteration of the fabric by rockfall impact. In sum, the magnetic characterization of the ash layers has shown the occurrence of different post-burning alteration processes previously not identified at the site. Alteration processes in prehistoric combustion features are often identified from macroscopic observations but our study demonstrates that multiple processes can affect them and are usually unnoted because they take place on a microscopic scale. Their identification is critical for a correct chronological and cultural interpretation of a site (e.g. collection of samples for dating, stratigraphic displacement of remains), especially if significant alterations are involved. Magnetic methods are therefore a powerful but underutilized tool in palaeolithic research for the identification and evaluation of taphonomic processes affecting prehistoric fires.

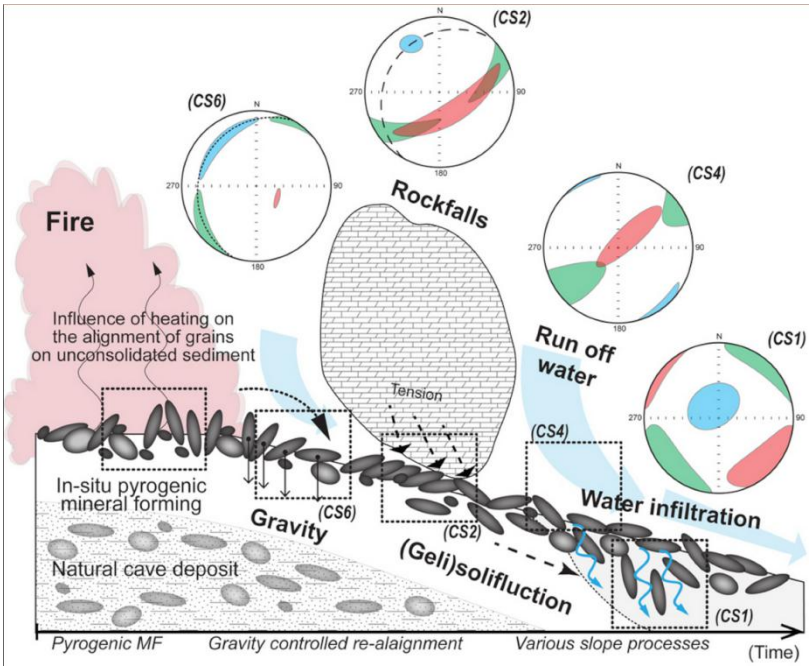

Figure 1. Combination of processes which may contribute to the development of the MF in anthropogenic burnt facies in cave successions. The ellipsoids on the stereoplots represent the theoretical alignment of the principal susceptibilities based on the 95 per cent confidence ellipsoids in the ash samples from Crvena Stijena succession (black—κ_{max}, dark grey—κ_{int} and light grey—κ_{min} ellipsoids).

10. 过去气候变化对未来的启示

翻译人：郑威　11930589@mail.sustech.edu.cn

Tierney J E, Poulsen C J, Montañez I P, et al. ***Past climates inform our future*** *[J]. Science, 2020, 370: 6517.*

https://doi.org/10.1126/science.aay3701

摘要：在全球变暖的背景下，提升未来气候变化的预测有非常深远的需求。尽管最新的地球系统模型提供了前所未有的大量特征，基本的不确定性继续笼罩我们对未来的视野。过去的气候只提供了观察地球系统对高二氧化碳浓度响应的机会，强调了古气候学在限制未来气候变化的方面的基本作用。在这里，我们回顾了和气候预测相关的古气候信息并讨论了新方法的前景以更好的从过去气候变化中得到启示。代用指标方法和解释的进步为利用过去的气候进行模型评估铺平了道路，我们认为这种做法应该被广泛采用。。

ABSTRACT: As the world warms, there is a profound need to improve projections of climate change. Although the latest Earth system models offer an unprecedented number of features, fundamental uncertainties continue to cloud our view of the future. Past climates provide the only opportunity to observe how the Earth system responds to high carbon dioxide, underlining a fundamental role for paleoclimatology in constraining future climate change. Here, we review the relevancy of paleoclimate information for climate prediction and discuss the prospects for emerging methodologies to further insights gained from past climates. Advances in proxy methods and interpretations pave the way for the use of past climates for model evaluation—a practice that we argue should be widely adopted.

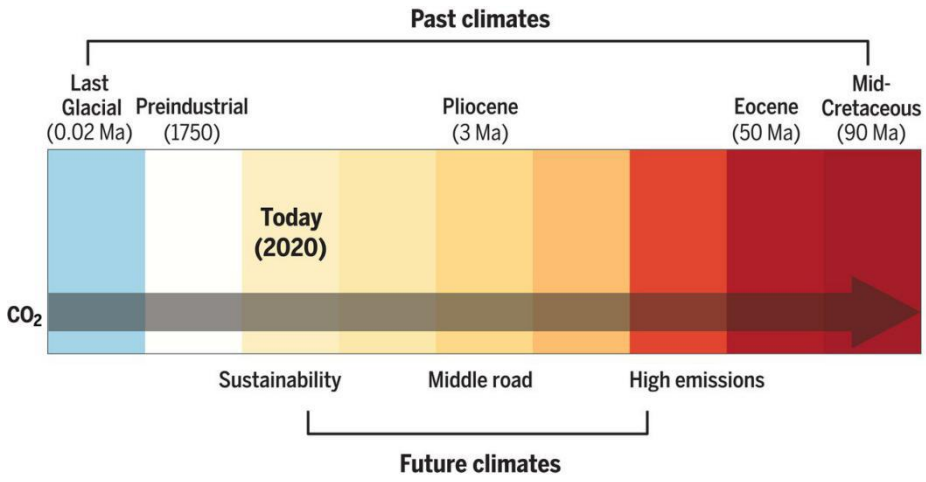

Figure 1. Past climates (denoted on top) provide context for future climate scenarios (at bottom). Ma= millions of years ago. Both past and future climates are colored by their estimated change in globalmean annual surface temperature relative to preindustrial conditions. “Sustainability”, “Middle road”,and “High emissions” represent the estimated global temperature anomalies at 2300 from the SharedSocioeconomic Pathways (SSPs) SSP1-2.6, SSP2-4.5, and SSP5-8.5, respectively. In both the past andfuture cases, warmer climates are associated with increases in CO_2.

11. 对磁铁矿和赤铁矿复杂混合物的磁信号分解技术的评估:犬山红燧石

翻译人：李海 12031330@mail.sustech.edu.cn

Hu P, Oda H, Zhao X, et al. ***Assessment of magnetic techniques for understanding complex mixtures of magnetite and hematite: the Inuyama red chert*** *[J]. Journal of Geophysical Research: Solid Earth, 2020, 125: e2020JB019518.*

https://doi.org/10.1029/2020JB019518

摘要: 磁铁矿与赤铁矿的混合物在自然界中广泛分布。对这些矿物进行磁学信息的分离，对于评估古地磁记录、提取地质及古环境信息等具有重要意义。由于赤铁矿的弱磁化及高矫顽力性质，使得难以从复杂的磁铁矿与赤铁矿的混合物中分离准确的磁学信号。本次研究，我们评估了 FORC 图、extended FORC 图、FORC 主成分分析（FORC-PCA）、IRM 曲线分解及剩余磁滞回线主成分分析在日本犬山红燧石样品中磁性信号分离的有效性。我们还使用 FORC-PCA 与 IRM 分解来分析红燧石中磁铁矿与赤铁矿的磁畴和矫顽力分布。结果显示，IRM 曲线分解可提供与矫顽力相关的组分信息，而 FORC-PCA 可以有效的识别磁畴状态。剩余磁滞回线的主成分分析指示了影响剩磁变化的最重要因素与微小矫顽力变化的信息。为了更好识别复杂的磁铁矿和赤铁矿混合物中的成分，建议使用剩余磁滞回线的主成分分析和代表性样品的 FORC 图分析来识别磁畴状态与矫顽力分布。

Abstract: Magnetite and hematite mixtures occur widely in nature. Magnetic unmixing of the signals recorded by these minerals can be important for assessing the origin of their respective paleomagnetic remanences and for extracting geological and paleoenvironmental information. However, unmixing magnetic signals from complex magnetite and hematite mixtures is difficult because of the weak magnetization and high coercivity of hematite. We assess here the relative effectiveness of first-order reversal curve (FORC) and extended FORC-type diagrams, FORC principal component analysis (PCA), isothermal remanent magnetization (IRM) curve decomposition, and PCA of remanent hysteretic curves for unmixing magnetic components in samples from the magnetically complex Inuyama red chert, Japan. We also further characterize the domain state and coercivity distributions of both magnetite and hematite with FORC-PCA and IRM acquisition analysis in the red chert. We show that IRM curve decomposition can provide valuable component-specific information linked to coercivity, while FORC-PCA enables effective magnetic domain state identification. PCA of remanent hysteretic curves provides useful

information about the most significant factors influencing remanence variations and subtle coercivity changes. To identify components in complex magnetite and hematite mixtures, we recommend PCA analysis of remanent hysteretic curves combined with FORC analysis of representative samples to identify domain states and coercivity distributions.

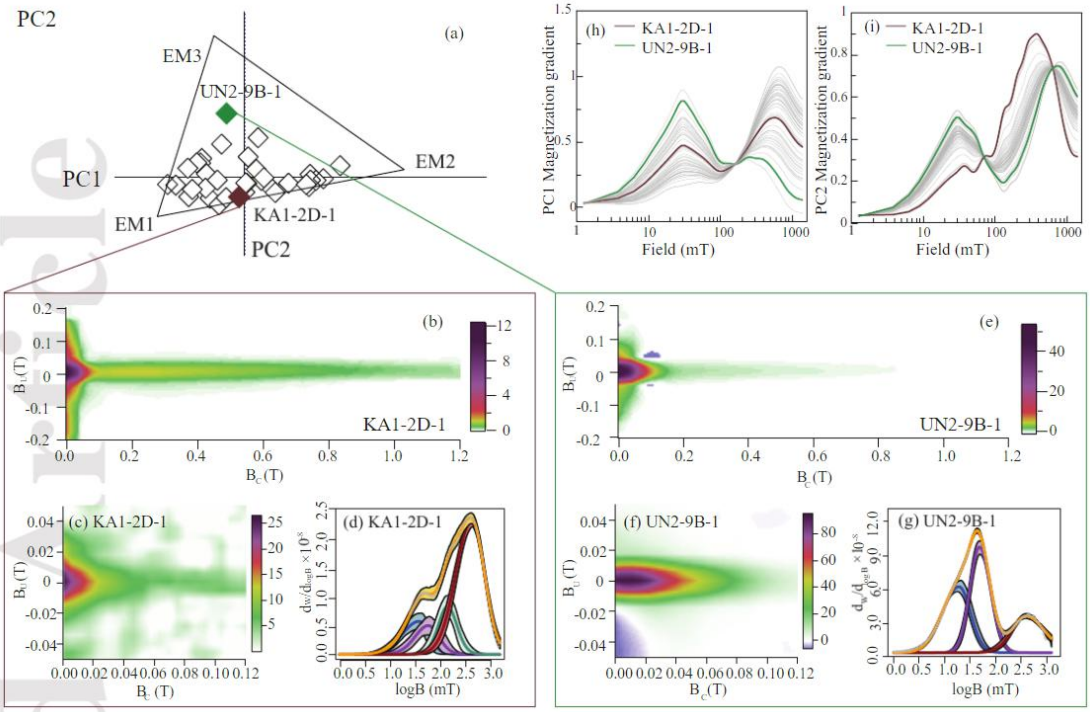

Figure 2. Comparison among FORC-PCA, IRM acquisition unmixing, and Mrh PCA results along the PC2 axis of the FORC-PCA solution. (a) PC space for the FORC-PCA solution; (b, e) reconstructed FORC diagrams using two PCs for the whole applied field range for samples KA1-2D-1 and UN2-9B-1; (c, f) reconstructed FORC diagrams using two PCs for samples KA1-2D-1 and UN2-9B-1 for the 0 to 120 mT range ; and (d, g) IRM acquisition unmixing results for samples KA1-2D-1 and UN2-9B-1. Blue, purple, green, and red lines represent components C1, C2, C3, and C4, respectively. The yellow line represents the total magnetization. (h, i) Magnetization gradient of PC1 and PC2 from Mrh PCA; brown and green lines represent results for samples KA1-2D-1 and UN2-9B-1, respectively.

12. 温带地区气候、构造引起的河流演变及岩溶作用和海平面变化的驱动关系

翻译人：周洋 zhouy3@sustech.edu.cn

Harmand D, Adamson K, Rixhon G, et al. ***Relationships between fluvial evolution and karstification related to climatic, tectonic and eustatic forcing in temperate regions*** *[J]. Quaternary Science Reviews, 2017, 166: 38–56.*

http://dx.doi.org/10.1016/j.quascirev.2017.02.016.

摘要：本文论述了河流演变与岩溶之间关系的多样性。强调了宇宙成因核素定年方法在研究分层洞穴通道中的沉积序列中的基本作用，为这些复杂的相互作用提供了新的认识。尽管喀斯特地貌在世界范围内分布广泛，但我们专注于欧洲的喀斯特地貌中沉积记录保存得特别好的地方。我们收集了河流沉积物的最新年代数据，以检验岩溶、侵蚀和沉积的时间。最完整的记录发生在构造抬升的高山上，含有一些可追溯到中新世的古老的沉积物。有证据表明，构造隆升、气候条件和河流动力学（例如，拐点后退、河道流量/沉积物荷载增加）都可以在洞穴成因和地貌演化中发挥重要作用。在蒸发岩中，成岩作用的特征是快速溶解和沉降。在欧洲流域，石膏洞穴的发展主要发生在气候比较寒冷的时期，而石灰岩洞穴则在温暖的冰期或间冰期形成。我们提出了四种河流和岩溶演化模型，进一步强调了研究的广阔前景。

ABSTRACT: This paper reviews the diversity of relationships between river evolution and karstogenesis. It also underlines the fundamental role of numerical dating methods (e.g. cosmogenic nuclides) applied to sedimentary sequences in tiered cave passages as they have provided new insights into these complex interactions. Although karst terrain is widespread worldwide, we focus on European karst catchments, where the sedimentary records are especially well preserved. We review the recent dating of fluvial sediments and speleothems, to examine the timing of karstification, incision and deposition in cave levels. The most complete alluvial records occur in tectonically uplifted high mountains where some of the oldest sediment fills date to the Miocene. Evidence indicates that not only uplift, but also climatic conditions and fluvial dynamics (e.g. knickpoint retreat, increased channel flow and/or sediment load, and stream piracies) can

play a major role in speleogenesis and geomorphological evolution. In evaporate rocks, speleogenesis is characterized by rapid dissolution and subsidence. In European catchments, gypsum cave development largely occurred during cold climate periods, while limestone caves formed during warm interglacial or interstadial phases. Our synthesis is used to propose four models of fluvial and karst evolution, and highlight perspectives for further research.

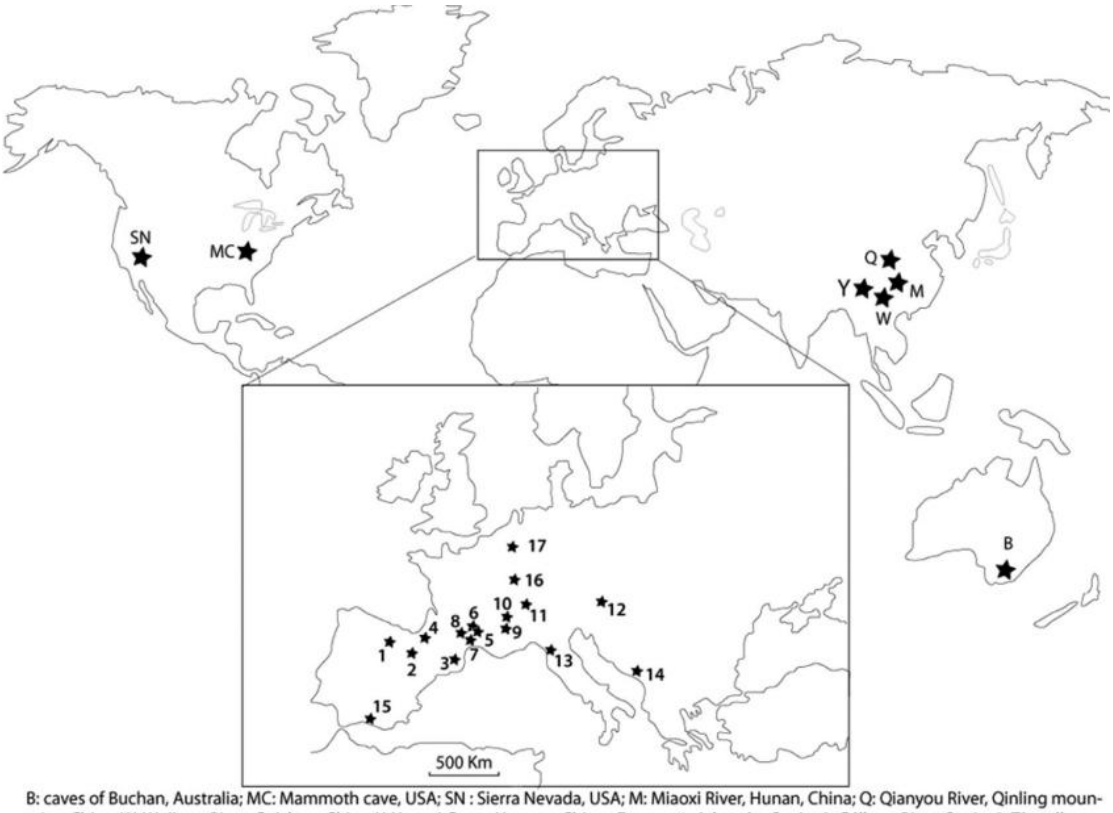

B: caves of Buchan, Australia; MC: Mammoth cave, USA; SN : Sierra Nevada, USA; M: Miaoxi River, Hunan, China; Q: Qianyou River, Qinling mountains, China; W: Wujiang River, Guizhou, China; Y: Yangzi Gorge,Yunnan, China; Europe: 1: Arlanzón, Spain; 2: Gállego River, Spain; 3: Têt valley, Eastern Pyrenees, France; 4: Pierre-Saint-Martin, Western Pyrenees, France; 5: Lower Ardèche valley, France; 6: Middle Ardèche valley, France; 7: Southern Larzac plateau, Grands Causses, France; 8: Tarn valley at Millau, Grands Causses, France; 9: Vercors, subalpine massif, France; 10: Mont Granier, Grande Chartreuse, subalpine massif, France; 11: Siebenhengste, Switzerland; 12: Mur valley, Eastern Alps, Austria; 13: Monte Corcia, Alpi Apuane, Italy; 14: Mount Orjen, Montenegro; 15: Gypsum karst of Sorbas, Spain; 16: Caves of Pierre-la-Treiche, Eastern Paris Basin, France; 17: Cave of Belle-Roche, Ardenne massif, Belgium

Figure 1. Location map of the karstic areas discussed in the text.

13. 来自南极 Erebus 大火成岩省上新世-更新世的地磁场古方向与古强度结果

翻译人：张伟杰 12031188@mail.sustech.edu.cn

Asefaw H A, Tauxe L, Koppers A A P, et al. ***Four-Dimensional paleomagnetic dataset: Plio-Pleistocene paleodirection and paleointensity results from the Erebus Volcanic Province, Antarctica*** *[J]. Journal of Geophysical Research: Solid Earth, 2020, online.*

https://doi.org/10.1029/2020JB020834

摘要：轴向地心偶极子场可以拓展到地质历史时期这是进行古地磁学研究的基础假设。0~5Myr 的全球的古磁场方向符合包含有小的非偶极子场，但是主要是轴向地心偶极子场控制的地磁场结构，然而同时期的古地磁场强度结果并非如此。在轴向地心偶极子模型中高纬记录的强度值应该更高，但是当前的数据库指示古强度值与纬度不相关。为了去确定南极洲相对低的古强度结果反应了当时的地磁场信息，或者是低质量的结果或是采样时间跨度不充分造成的结果，因此我们在南极洲展开了新的地磁场信息研究。本研究聚焦于上新世-更新世地磁场特征研究。综合分析了 Erebus 大火成岩省新得到的与已经发表的古地磁场方向与古地磁场强度结果。利用热退磁和交变退磁从 98 个采样点得到了古地磁场方向结果。利用修改后的 IZZI Thellier-Thellier 方法从 26 个采样点得到古强度结果。得到的古地磁极（201.85°，87.65°）与α95（5.51°）支持轴向地心偶极子场假设，同时虚地磁极的分散程度也符合 TK03 长期变化模型的不确定度。我们得到的时间平均的地磁场强度结果 33.57±2.71μT 是明显更弱比通过现今评估得到的期望的轴向地心偶极子场模型。。

ABSTRACT: A fundamental assumption in paleomagnetism is that a geocentric axial dipole (GAD) geomagnetic field structure extends to the ancient field. Global paleodirectional compilations that span 0-5 Myr support a GAD dominated field structure with minor non-GAD contributions, however, the paleointensity data over the same period do not. In a GAD field, higher latitudes should preserve higher intensity, but the current database suggests that intensities are independent of latitude. To determine whether the seemingly “low” intensities from Antarctica reflect the ancient field, rather than low quality data or inadequate temporal sampling, we have

conducted a new study of the paleomagnetic field in Antarctica. This study focuses on the paleomagnetic field structure over the Plio-Pleistocene. We combine and re-analyze new and published paleodirectional and paleointensity results from the Erebus volcanic province. to recover paleodirections from 98 sites that were both thermally and AF demagnetized and then subjected to a set of strict selection criteria and paleointensities from 26 from the Plio-Pleistocene) sites that underwent the IZZI modified Thellier-Thellier experiment and were also subjected to a strict set of selection criteria. The paleopole (201.85°, 87.65°) and α95 (5.51°) recovered from our paleodirectional study supports the GAD hypothesis and the scatter of the virtual geomagnetic poles falls within the uncertainty of that predicted by TK03 paleosecular variation model. Our time averaged field strength estimate, 33.57 μT ± 2.71 μT, is significantly weaker than that expected from a GAD field estimated by the present field.

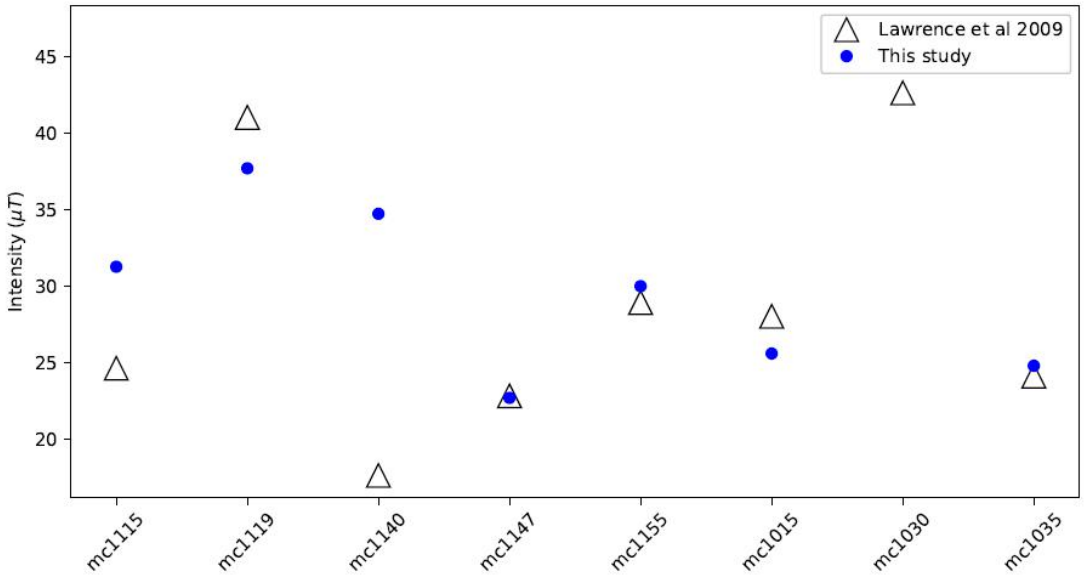

Figure 1. Average intensity estimates for the sites in this study that passed CCRIT (blue circles) and the sites from Lawrence et al. 2009 (white triangles) that passed their set of selection criteria.